How the Grassland Got Its Stripes: Periodic *Bouteloua gracilis* death in self-organized banded vegetation patterns

A Thesis

Presented to

The Faculty of the Department of Environmental Studies and Science
Colorado College

In Partial Fulfillment of the Requirements for the Degree
Bachelor of Arts

By
Paige Simenz
May 2024

How the Grassland Got Its Stripes:
Periodic *Bouteloua gracilis* death in self-organized banded vegetation patterns

By Paige Simenz

Abstract

Arid grasslands represent 12.5% of North American land cover and blue grama grass (*Bouteloua gracilis*) is the dominant species in cover and primary production on this landscape. In the shortgrass steppe of eastern Colorado, blue grama has experienced a significant biomass reduction in conjunction with several significant droughts beginning in 2002. Our study site at Chico Basin Ranch (in between Pueblo and Colorado Springs, CO) developed a self-organized banded vegetation pattern over the same temporal scale. Self-organized vegetation patterns often present in landscapes experiencing adverse conditions as a mechanism of optimizing water management so that bare patches streamline incoming water flow towards vegetated patches. Using on-the-ground land cover surveys and a comparison of NDVI from 2023 and 2020 aerial images, this study seeks to determine that this pattern is formed by periodic bands of dying vegetation. Aggregate mean data from transect land cover surveys reveals an overall system trend of two living grass coverage peaks on either side of the transect, and three offset peaks in between with senescing grass cover peaking first, then dead grass, and finally bare ground. The statistically significant relationships between adjacent land cover peaks at various spatial lags indicates the overall direction of the system with the downslope edges of groves dying and eventually eroding to bare ground. Taken individually, survey transects can be broadly sorted into categories based level of vegetation organization within the pattern framework: Type I "messy" transects, which present an inverse relationship between interspersed living and dead grass patches, Type II which have developed a distinct band of upslope living grass and a downslope dead grass band, and Type III in which a portion of the downslope dead grass band has eroded to bare ground. Analysis of NDVI change from 2020 to 2023 reveals how these stripes develop over time, with growth remaining concentrated on the upslope edge of vegetated bands and declining grass health or density remaining on the downslope edge of vegetation, underlining the pre-existing pattern. Based on these results, we conclude that the banded pattern is formed by concentrated blue grama growth along the upslope edge of vegetated bands, with the remaining downslope grass bands eventually dying and eroding to bare ground. This pattern is self-perpetuating, as over the past three years, grass presence has facilitated further growth and grass loss led to a less suitable surrounding habitat. While there are research gaps in blue grama mechanisms of senescence and death in response to drought, it is likely that these periodic patterns of death were initiated by the compounding effects of unusually long-term drought.

Introduction

Observed around the world, self-patterned vegetation systems in arid ecosystems represent a community-level response to limited water. By self-organizing vegetation into spotted or striped patches, the incoming water is redistributed via sheetflow over bare patches onto downslope concentrated vegetated patches. By doing so, ecosystems ultimately support more biomass than possible in a spatially random homogeneous full-vegetation cover state (Reitkert et al. 2002; Dunkerly 2018). While the bare soil patches have low infiltration and high evaporation rates, they effectively funnel incoming precipitation into established vegetation patches which are able to efficiently intake the water due to higher surface roughness and porosity from the roots, and canopy shading via leaves to reduce surface evaporation and increase infiltration (Dunkerly 2018). The formation process of such patterns must include both a building phase—in which plant life concentrates and thrives in one area—and a degenerative phase—through which overall plant cover decreases as individuals in between vegetated patches die out (Aguiar & Sala 1999). In strongly water-limited ecosystems, plant cover is typically under 60% regardless of patterned organization (Aguiar & Sala 1999). By concentrating remaining vegetation into dense clumps or stripes, the plant community is able to most effectively make use of the crucial resource.

To understand the increased ecological efficiency of patterned vegetation, it is useful to consider the ineffective precipitation, or zero-yield, parameter describes how redistribution via sheetflow decreases an ecosystem's precipitation threshold by allocating all incoming water towards established vegetation patches while the run-off patches, already unable to maintain vegetation, yield no further consequence from further water shortage (Noy-Meir 1973). This reallocation artificially increases water intake within the vegetated patches to a range that can sustain plant life in an ecosystem which would otherwise not (Aguiar & Sala 1999). These vegetated patches continually sustain themselves through positive feedback systems, by which plant growth enables improved water catchment, and thereby further promoting plant growth. Turing's (1952) Activator-Inhibitor principle provides additional theoretical groundwork for self-patterning systems through the lens of scale-dependent feedback loops. As organisms modify their environment through positive feedback loops to improve local conditions—in this case, artificially heightened water availability—they inherently inhibit growth and establishment at a larger distance where their impact becomes inhibitive (Rietkerk & van de Koppel 2008). Band growth is ultimately limited by a long-distance inhibitive positive feedback loop as the ecosystem is less efficient at maintaining water, and thereby less habitable for plants, at further distances from the densely vegetated patches.

Pattern formation is generally observed in adverse environmental conditions which necessitate resource concentration to manage a limiting resource (Rietkerk & van de Koppel 2008). Often these two patterned systems develop at the threshold when two attracting alternative states are possible, each of which could prevail through positive feedback loops (Rietkerk et al. 2004). In the case of banded vegetation, the two ulterior states are homogeneous fully vegetated or homogeneous bare; the landscape may initiate pattern formation to maximize water use efficiency as a last defense when water yields decrease below the needed amount to maintain full-cover. Rietkerk et al. (2004) describe the patterning observed in arid landscapes as a hysteresis, by which it only arises when resource availability is decreased. With bare soil too hostile for establishing new growth, once assumed this patterning does not easily reverse.

Therefore, self-organization can act as a precursor for catastrophic ecosystem shifts as it emerges only when the system exists at an existentially threatening resource threshold (Rietkerk et al. 2004). Often, such catastrophic shifts are associated with long-term climate changes when the ecosystem is presented with a new precipitation regime insufficient for maintaining the current vegetation structure. Chen et al. (2015) describe that when climate change occurs over a sufficient time period, the ecosystem can adjust with resilience-promoting reorganization—such as banded vegetation patterns—which establish a new tipping point for collapse and vegetation may still persist with reduced water. If the change proceeds rapidly, however, vegetation does not have time to reorganize and the system accelerates towards ecological collapse, ultimately resulting in desertification (Fig. 1).

Areas of self-patterning vegetation have been primarily studied in arid regions of Australia and Africa (Dunkerley 2018). However, patterns have also been emerging in the arid grasslands of North America (Nasvik 2021) in the wake of long-term drought conditions. Grasslands represent 12.5% of North American land cover and provide crucial resources for agriculture (Evans et al. 2011). Despite drought events occurring naturally throughout the history of North American plains, several studies have found risk for ecological devastation with limited recovery following both unprecedented severe and long-term droughts, which are expected to become more prevalent under the incoming climate regime (Evans et al. 2011; Rondeau et al. 2017). Even when vegetation is maintained throughout these disruptions, they often constitute a significant change in the dominant vegetation which interrupts grazing cycles and overall ecosystem function.

Historically, blue grama grass, *Bouteloua gracilis*, has dominated land cover in the North American grasslands. Blue grama is not only the most important forage species as a nutritious food source for livestock and other grazers even during senescent periods, it is long adapted to withstand both grazing and drought stress (Sims et al. 1973). This C_4 warm-season grass has high water use efficiency and the potential to form a mat cover or present as a bunchgrass, holding 85% of root mass in the upper 20 centimeters of the soil (Smith et al. 2004). This upper-level root mass allows for quick response to the pulse-precipitation typical in arid grasslands, using pre-existing roots to absorb water immediately and taking advantage of the water influx to grow new roots over the following days, effectively expanding root surface area and water absorption potential (Lauenroth et al. 1987). Above-ground mass is primarily constituted of short cumless vegetative shoots with relatively few reproductive shoots, providing great resilience to grazing as little necessary biomass is lost (Smith et al. 2004; Eneboe et al. 2002). However, reproduction primarily via lateral tillers and short rhizomes presents issues for recolonization on bare ground once pre-established vegetation is lost. Reliance on adventitious roots complicates the establishment of blue grama seedlings, and therefore natural regeneration and complete recovery after severe disturbance may require at least 50 years (Smith et al. 2004). Additionally, C_4 grasses tend to present an overall decreased growth rate and produce smaller seeds with less endosperm and water storage, resulting in lower germination success during stressful conditions (Qi & Redmann 1993). Given the challenges for blue grama grass to recruit on bare ground, persistence of established clones is crucial.

Despite resilience towards drought stress, Evans et al. (2011), Rondeau et al. (2013), and Rondeau et al. (2017) have all empirically found significant loss of blue grama cover following

both severe acute and extended drought conditions. Such extreme conditions disrupt the root dynamics primarily responsible for blue grama's ability to quickly respond to incoming precipitation (Lauenroth et al. 1987). Evans et al. (2011) experimentally found these mechanisms can persist even under extremely long periods of resource limitation, yet after eight years of precipitation reduction the study plot began to reveal consequences. In these studies, even when blue grama is replaced by ruderals, the ecosystem dynamics are greatly altered as other incoming species are less nutritious for grazers and may present less long-term resilience (Evans et al. 2011; Rondeau et al. 2017).

In El Paso County, Colorado—an area predominantly composed of arid grassland— there has been an upward linear trend in daily temperature onsetting around 1995-2005 in El Paso County. While lacking a distinct linear trend, analysis of precipitation data suggests variability shifting towards stronger droughts over the past 20 years (Nasvik 2021). Increasing base temperatures increase evaporation rate and therefore heighten plant water needs, regardless of specific drought periods. However, the most recent drought periods in the area—some of the driest on record—occurred in 2002, 2012, 2018, and 2020 (Colorado Climate Center). Rondeau (2013) monitored vegetation cover at a study site in Pueblo, Colorado throughout the earliest pre-drought period, extreme drought, and recovery from 1999-2010. 2002 presented the most severe single-year drought in the region over the past century and resulted in up to 40% decline in blue grama coverage with an increase in shrub coverage; even seven years following, recovery to pre-drought levels was not evident. Given the long-observed extreme resilience of blue grama grass on the North American plains and its importance for agriculture and ecosystem functioning, population decline following expected accelerated drought and temperature conditions under the incoming climate region is certainly cause for concern.

An analysis of high-resolution aerial imagery at nearby Chico Basin Ranch in El Paso County, Colorado, found a significant increase in self-organized banded vegetation patterns over the time period from 1999-2019 (Nasvik 2021). While change in overall grass coverage has not been well established at this site, it is reasonable to suppose that it has decreased similarly to the plot monitored by Rondeau (2013) and this change may be connected to emergent patterning as it lies only 10 kilometers away. Significant banded patterns were found in low proportions of the Chico Basin Ranch study area preceding the most extreme drought in 2002, yet saw a 20% increase throughout the following two decades. While patterning demonstrated a delayed emergence in the years following the 2002 drought, it was not until 2015—presumably in a delayed effect from the 2012 dry periods—that the bands solidified and the regime appeared unaffected by proceeding dry periods. Beyond the distinctly banded portions of the study site, image analysis revealed that all vegetation is self-organizing to some statistically significant degree beyond complete spatial randomness.

Microhydrologic experiments at Chico Basin Ranch have also confirmed the development of self-organized banding patterns, finding water reallocation and formation mechanisms consistent with those previously described; as sheetflow moves downslope across the bare patches, water begins to pool and infiltrate upon reaching vegetation patches with greater surface roughness and elevation (Sticpewich 2022). This study also included an unprecedented finding in how pools formed between grass bunches within vegetated bands may also contribute to the water conservation as they remained up to 20 minutes following water input. These findings

complement the findings of Nasvik (2021) in demonstrating that emerging patterns are distinctly tied to water management, and likely a response to the preceding dry periods which have been associated with decreased grass coverage in the region.

Given the advancing pattern formation at Chico Basin Ranch, this study site presents an example of how an arid grassland on the North American plains—even while suffering overall loss in grass coverage—can acclimate to a new precipitation regime through self-organization when the change occurs sufficiently gradually, effectively lowering the critical water-need tipping point to avoid total collapse (Chen et al. 2022). However, empirical studies such as Evans et al. (2011) and Rondeau (2013) argue that even extremely drought-tolerant organisms have limits and expected drought conditions may surpass their stress tolerance limits. Landscapes displaying self-organized patterns present important study sites for resilience mechanisms, as they exist on a threshold of resource availability, already too limited to maintain previous levels of coverage (Rietkerk et al. 2004). Given historical and continuing drought conditions in the region and the distinct arisal of banded patterns, further studies at Chico Basin Ranch can deepen understanding of the mechanisms behind and future implications for self-patterning vegetation as a response to water scarcity. This paper seeks to build upon previous studies to better understand the mechanisms of pattern formation—specifically expanding upon the observation of dead grass heads in the spaces between the bands to postulate the pattern is formed by spatially periodic grass death—using both spatial imagery analysis and fine-scale land cover analysis.

Methods

Site Description

This study was conducted on Chico Basin Ranch, a cattle ranch on the border of El Paso County and Pueblo County, Colorado (Fig. 2). Owned by a public land trust, Chico Basin Ranch practices holistic resource management for supporting grazing cattle and promotes educational opportunities. This area constitutes an arid grassland ecosystem east of the Rocky Mountain foothills. This site receives approximately 10-15 inches of precipitation annually, with severe drought years in 2002, 2010, 2012, 2018, and 2020(Colorado Climate Center; Nasvik 2021). This site presents banded vegetation patterns, which have been increasing in prevalence over the past decade (Nasvik 2021).

The shortgrass prairie is dominated by Blue grama grass (*Bouteloua gracilis*), a drought-resilient and nutrient-rich grass commonly used for cattle grazing. This grass has experienced decreasing coverage within the region over the course of preceding drought years; Rondeau et al. (2016) observed a 62% decrease from 1999-2015 at a study site approximately 25 kilometers away. At our fieldsite this decline of grass coincided with the development of the banded patterns of interest (Nasvik, 2021). Buffalo grass (*Bouteloua dactyloides*) is also highly present in the area, along with Cholla cactus (*Cylindropuntia*) growing periodically throughout the site (Nasvik 2021); our data collection sites generally avoided Cholla. In the past few years, invasive tumbleweed (salsola, *Salsola tragus*) has aggressively encroached on the upslope side of the grass patches (or, downslope edge of the bare spots) over the year preceding this study.

Data collection occurred on an approximately 200 meter x 90 meter plot (coordinates: 38.5131833˚, -104.4222770˚) immediately east of the ranch's airstrip and south of the hangar. This area is generally flat, with a gradual north-south downward slope. (Fig. 3). All data collection occurred from September 25-October 18, 2023 at the end of a particularly wet growing season. The last preceding rain occurred approximately three weeks prior to the field collection and the whole field site had a mixture of green active grass and grass that has already senesced and was gray-brown in color.

Field Sampling

Land Cover Survey

We marked out 20 transects with flagging across distinct wavelengths of various lengths within the study site. One wavelength was defined as the approximate mid-section of the upslope vegetated patch (hereafter, grove) across the bare patch (hereafter, intergrove), to the mid-section of the downslope grove. Through the entire wavelength, we placed 0.5 meter x 0.5 meter quadrat survey squares along a straight line through the widest part of the intergrove. Within each quadrat, we counted the number of living tumbleweeds, dead tumbleweeds, heads of senescing grass, and heads of dead grass. Senescing grass maintained fairly dense blades which presented in dull brown or gray, whereas dead grass heads were defined by a remaining raised structure of exposed abraded underground rhizomes perched on dead roots and which may have stalks, but no leaves. Due to the complexity in structure of the dead rhizomes—which may be densely branched or apparently singular—we used a circular kernel size with 0.25 centimeter diameter to count whether dead grass and senescing grass were present. We also took photos of each quadrat for future analysis.

We digitally added 11x11 grids with 100 intersections to the photos of each quadrat to determine percent coverage of living grass, dead grass heads, living tumbleweeds, dead tumbleweeds, litter, and bare ground (Fig. 4a-c). At each intersection point, we marked which of the preceding land cover types was present.

This meant that we had two metrics that indicated the prevalence of dead grass heads: percent cover determined from the photographs, and number of kernels containing a dead grass head or senescent grass counted in the field. Ultimately, land cover data analysis utilized field-count of kernels with dead grass and number of senescing grass heads. The choice of using the field count over the percent cover was because the three dimensional structure of the living grass in some cases obscured the presence of dead grass. The two metrics (field count and percent cover) were significantly positively correlated ($p<0.001$).

Aerial Imagery

6-band aerial imagery of the entire study site was captured using a Inspire 2 drone with an Altum Professional Multispectral/Thermal/High-Resolution Sensor Kit by Micasense with 6 bands: red, green, blue, near infrared, red edge, and thermal. The drone was flown at 13m elevation in a "lawnmower pattern" with 85% side lap and 85% in-line overlap. The flight necessitated three battery changes and at the initiation of each flight we took photographs of calibration reflectance panels.We placed GPS points at highly visible cacti using a Trimble Geoexplorer 6000 GPS to collect geographic control points (GCPs). The GPS was differentially corrected in Geoexplorer software and the corrected points had mean error of 15 cm Images were processed with GCPs in AgiSoft Metashape Professional to create the final 6-band orthomosaic located with a mean error of 0.16 meters (0.32 meter maximum) based on Agisoft Metashape accuracy report.

Data Analysis

Aerial Images

A 29 meter x 43 meter area of interest (AOI) within the study site containing several clearly defined vegetation bands was selected to compare with a historical study image from 2020. While the 2020 image was previously processed and analyzed for Normalized Difference Vegetation Index (NDVI) using ArcGis Pro (Kummel Lab), both images were uploaded to ArcGis Pro for further comparative analysis. After clipping the images to the same selected area of interest, we used prominent cacti for georeferencing with a mean 0.059 meter error (maximum: 0.087 meters). In order to allow direct comparison while accounting for error, pixels for both images resampled to a common pixel resolution of 0.25 meters and having the pixels directly aligned. After calculating 2023 NDVI, we tested differing symbology classifications to best determine values for grass with the highest and lowest NDVI while minimizing inclusion of cacti and bare ground. In the 2020 image the highest values corresponding to grass was 0.32 and the lowest was 0.18, and in the 2023 image 0.39 was the highest value for grass and 0.09 was the lowest. With the grass' NDVI range determined, we normalized the datasets on a scale of 0 to 1, 0 representing grass presenting with lowest NDVI and 1 representing grass with the highest. We used the regression equations for the minimum, maximum, and mean values of each index ($y = 7.1429x - 1.2857$ for 2020; $y = 3.3333x - 0.3$ for 2023) to reassign the datasets with normalized values using the Raster Calculator; in both datasets, values less than zero or greater than one (representing cacti or bare ground) were set NULL.

This scaling removed bare ground as the bare ground had lower NDVI values than the lowest NDVI corresponding to grass, and cacti because cholla cacti had consistently higher NDVI than the highest NDVI corresponding to grass. Tumbleweeds were removed when possible but presented a greater challenge because they had an NDVI signature sometimes indistinguishable from healthiest grass.

With data normalized, we subtracted the 2020 dataset from 2023 so that a negative value for a pixel represented grass with decreasing NDVI (orange and red coloring), and a positive value

represented increasing NDVI (green coloring) to determine changes in grass density and health across the AOI over the past three years.

Statistical Analysis

Land Cover

In order to statistically test the relationship between presence of living grass and dead grass in 2023 field transects, we initially ran all data living grass and dead grass points from each transect through cor.test in RStudio for a Pearson's correlation coefficient.

To further reveal the overall trend revealed by the land cover survey, we conducted a lagged correlation analysis on mean land cover across a spatially normalized transect. In order to directly compare transects of different lengths, we divided the quadrat number by total number of quadrants within the respective transect to determine proportional spacing, resulting in values of 0 to 1, with 0 being the approximate mid-section of the upslope grove and 1 representing the mid-section of the downslope grove. Using these proportional location values, we created bins at intervals corresponding to 5% of the transect length—making every interval of 0.05 (inclusive of the upper value)—and calculated the mean value for each land cover type within the bin; for plotting, mean values of land cover were placed at the bin's midpoint (for example, the mean values for the 0-0.05 bin were placed at 0.025). With the average values for each land cover type plotted along the normalized transect, we ran Pearson's Correlation tests (using cor.test function in RStudio) at seven spatial lags for each pair of land cover types with adjacent peaks: living grass-senescent grass, senescent grass-dead grass, and dead grass-bare ground. This provided a metric for assessing the magnitude of displacement for each peak in land cover, with each spatial lag representing 10% of the transect. See Appendix 1 for the full R code loop.

Aerial Imagery

In addition to visual analysis, we used a Pearson's correlation test to determine statistical significance of NDVI change across groves from 2020 to 2023. To generate numeric NDVI change data, we placed five rectangular transects in ArcGis Pro of varying lengths across well-defined groves, and divided them into 1 meter x 0.5 meter quadrats. The Zonal Statistics as Table feature extracted maximum, minimum, and mean values of NDVI change from each quadrat; we exported this data to Microsoft Excel and manually placed them in the correct order from upslope to downslope. Finally, we ran data for each transect through the cor.test function in RStudio to determine correlation between the paired samples of quadrat location and change in NDVI.

Results

Land Cover Analysis

Analysis of finescale land cover data reveals the vegetative makeup and organization of the landscape as it continuously transitions towards a patterned regime. Aggregate data from all 20 transects quadrat proportion covered by living grass versus number of kernels with dead grass

heads reveals a statistically significant negative correlation (r=-0.386, n=373, p=1.211e-14). Ecologically, this indicates that bare patches likely originated from previous grass death. The relationship is best described as an envelope relationship where for each percent covered by living grass, the dead grass varies from zero to a maximum value, and the maximum number of dead grass kernels is a decreasing function of percent grass cover. Ecologically speaking, there are areas with neither living grass nor dead grass heads (i.e. bare ground), and there are areas in which they are both present at intermediate to low levels, but there are no spaces in which both living and dead grass densely cover the quadrat (Fig. 5). Statistically this envelope-type relationship can originate from two different mechanisms. First, the proportion of living grass sets the maximum dead grass that can be observed, and another variable determines the value of dead grass between zero and the maximum. Second, the spatial structure of the progression of living and dead grass along each transect is such that one's peak cover lags behind the other at various lags in each transect. Transects with low lags produce the edge of the envelope while transects with high lags produce the data points in the interior part of the envelope. To distinguish between the two we need to examine the spatial structure of the sequence within each transect.

When plotted together over a spatially normalized transect (using bins representing relative proportional positioning of each data point rather than quadrat number), the figure reveals a U-shaped progression of living grass cover, and within the "U" there are three lagged peaks with senescing cover peaking first, then dead grass, and finally bare ground peaking last (Fig. 6). Statistically, lag correlations reveal a significant relationship between each pair of adjacent land cover peaks at different spatial lags; the peaks of living and dead grass are displaced at a lag representing 70% of the transect (r=0.872, p=4.799e-05), senescent and dead grass maximize correlation at a 10% lag (r=0.918, p=3.12), and dead grass and bare ground peak maximize correlation at a 20% lag r-=0.927, p=3.15e-08 (Table 1). Thus, we can conclude that the envelope relationship between living and dead grass is formed by various spatially lagged peaks in each type of land cover, which reveal the overall direction of the system with the downslope edges of groves dying out and eventually eroding to bare ground.

Fine scale analysis of individual transects from 2023 field surveys shows that the transects can be broadly divided into three different categories based on pattern development between living and dead grass, and bare ground (senescing grass presents a less consistent relationship, so this variable will be discussed in a separate section). Type I displays a relatively low level of organization, with living and dead grass still presenting a generally inverse relationship, but patches of living and dead are interspersed rather than located within a singular band of each. Of the 20 transects, only four transects (T1, T16, T13, T20) belong to this category. To illustrate this pattern we chose one representative transect; Transect 16 (Fig. 7a), which clearly displays this type of high variability and low organization of the grass cover as one moves from the uphill grove through the intergrove to the downhill grove. Here living grass coverage peaks on the upslope side of the transect, reaching around 65% cover in Quadrat 2. After peaking, living grass drops sharply to 0% by Quadrat 7. As living grass coverage is dropping, dead grass coverage climbs from 5 kernels early in the transect to nearly 30 in Quadrat 5. Both living and dead grass counts drop below 10 at Quadrat 7 where bare ground is the dominant land cover of the three. The point which differentiates Type one is the second peak and drop of living grass, which spikes again to just under 30% in Quadrat 8, with bare ground also reaching 35% coverage. Living

grass and bare ground drop below 10% and there are less than 10 dead grass heads at Quadrat 10; areas such as these are commonly dominated by tumbleweeds, which are not included in this analysis. Living grass spikes back up to 50% at Quadrat 12, with both bare ground and dead grass remaining around 10 in their respective metrics. See Appendix 2a for all transects sorted into Type I.

Type II transects display a strong inverse relationship between living and dead grass, but without significant portions of bare ground. Figure 7b displays this development of patterning in transect 11, with living grass cover beginning around 70% and quickly dropping to 0% by Quadrat 7. Dead grass and bare ground presence both begin climbing around Quadrat 3, while living grass cover is dropping. Dead grass peaks at Quadrat 7 with a value of 30, slightly before bare ground with 70% coverage in Quadrat 10. Both land cover types drop starkly after Quadrat 11, and living grass dominates for the rest of the transect, peaking again around 70% in Quadrat 15. Six out of 20 transects were sorted into this category (T5, T7, T11, T15, T18, T19); see Appendix 2b for all transects sorted into Type II.

Type III transects represent the final observed stage of pattern development, presenting a similar living and dead grass relationship as Type II, but also featuring a primarily bare patch at the downslope edge of the intergrove (Fig. 7c). Living grass dominates coverage around 70% until Quadrat 5, with both bare ground and dead grass remaining around 20 in their respective metrics. As living grass drops sharply to 0% beginning around Quadrat 5, both dead grass and bare ground coverage begin climbing. Dead grass peaks at 60 in Quadrat 7, and then sharply drops, remaining just above 10 heads for the rest of the transect. Bare ground coverage continues climbing to peak at 60% in Quadrat 9. The land cover is primarily bare ground until it drops back to around 35% after its peak and living grass cover dominates for the remainder of the transect. 17 out of 20 transects surveyed display dead grass peaking before bare ground, but this trend is most notable within Type III. This was the largest category, with 10 out of 20 transects; see Appendix 2c for all transects sorted into Type III (T2, T3, T4, T6, T8, T9, T10, T12, T14, T17).

Senescence

Senescing grass patterns overall align with the broader land cover survey analysis, peaking on average between living grass and dead grass. The direct (not-lagged), marginally statistically significant negative correlation between living and senesced grass ($r=-0.428$, $n=20$ $p=0.06$) suggests that scenescense is not interspersed inn living grass cover, but rather that senescence happens in larger areas en-masse. The peak of senesced grass lags behind the living grass suggesting that the mass senescence happens downslope of the living grass grove. Likewise, the direct, not lagged, statistically significant negative correlation between the senesced and dead grass ($r= -0.795$, $n=20$, $p<0.001$) suggests that grass death does not happen interspersed in the senesced grass, but rather en-mass in distinct areas. The lagged correlations suggest that the grass death happens downslope of areas that show early senescence. In our Type I (“messy”) transect (Fig. 7a), senescing grass has two peaks of approximately 40 kernels at Quadrat 6 and 55 kernels at Quadrat 8; between the two peaks it drops down to 0. Throughout the rest of the transect, it typically peaks shortly after (or, downslope of) living grass around 20 kernels, and alternatively falls to 0. In the representative Type II (“ordered”) transect (Fig. 7b), senescing grass has a very clear peak at 22 kernels in Quadrat 4 as the initial living grass peak is falling, and then remains at 0 kernels through Quadrat 18, and does not exceed 10 kernels for the remainder of the transect.

In our Type III ("bare patch" transect (Fig. 7c), senescing grass climbs to a brief peak at 20 kernels in Quadrat 6 and quickly gives way to dead grass, remaining near 0 for the rest of the transect. While it does reveal a clear spatial pattern in our most representative transects, senescing grass presents less distinct peaks and troughs in each transect (and sometimes only marginally statistically significant negative correlations) relative to the other land cover types analyzed. Therefore, this variable has been included in the overall discussion of land cover types to consider its place within the pattern as the transition between living and dead grass, but excluded from plots of individual transects.

NDVI Change Analysis

We can determine how these spatial patterns continue to develop overtime in respect to growth and decay based on a qualitative visual analysis of the NDVI change map from 2020 to 2023 (Figure 4). Please note that the NDVI change was created by subtracting 2023 NDVI from 2020 so that negative values indicate decreasing density or health and positive values indicate increasing (see methods section for details). A visual qualitative analysis of the resulting map determined grass has been losing health or decreasing in density on downslope edges of groves (represented with red and orange pixels in Fig. 8), and generally increasing health or density along the upslope edge of the groves (represented with green pixels in Fig. 8). Areas of greatest grass growth form nearly parallel bands which stretch from the northeast corner of the AOI to the southwest, generally occurring along the top edge of groves. Areas of greatest NDVI decline are frequently clustered along the downslope edge of groves, with red likely representing death through greatest decline in NDVI; even if they still retain grass cover, such bands generally align with previously existing intergroves and their health decline indicates the continuation or solidification of the banded pattern.

The qualitative analysis is somewhat complicated by the presence of invasive tumbleweeds. Patches composed of uniformly dark green constitute tumbleweeds which typically recruited on the upslope edge of the grow. Some tumbleweeds could not be well-enough distinguished for removal based on NDVI signature, but their location is apparent based on the high resolution orthomosaic and this allowed us to exclude them from qualitative and quantitative analyses of the map. In Figure 8 the dense tumbleweed areas are marked by a pink outline.

To quantitatively test the significance of this relationship between grass position within grove and NDVI change, we identified five transects displaying this qualitatively observed pattern to different extents (labeled A-E in Fig. 8); each transect connects two adjacent intergroves through the intervening grove and avoided the presence of tumbleweeds. Statistical analysis of each transect reveals a negative correlation where the NDVI change index switches from positive (increased density or health) at the uphill side of the grove to negative (decreased health or density) at the downhill side of the grove; of the five transects this pattern was statistically significant in three (Fig. 9a-e, see Table 2 for full statistics)**.** Based on the categories previously determined by the land cover survey data, these transects can also be sorted into stages of development to represent how each may progress overtime. Transect E can be representative of a Type I ("messy") transect currently without distinct bare stripes, but still displaying statistically significant decline in NDVI along the downslope edge over the past three years ($r=-0.77$, $n=15$ $p=0.00083$). A band of red and orange pixels runs perpendicularly to the transect along its bottom edge, indicating the process of continuing intergrove formation. Transect B is

representative of Type II ("ordered"), with a statistically significant decrease in NDVI along the transect's downward slope (r=-0.78, n=13, p=0.001), but with a greater proportion of orange pixels than red (less severe decline in greeness). Lying between two well-defined intergroves, this transect has experienced loss in greeness along its bottom edge throughout the temporal scale, but likely not notable amounts of death resulting in new bare patches. Transects A, C, and D are representative of Type III ("bare patch") as groves lying between distinct intergroves with dense patches of greatest NDVI decline—likely resulting in increasing bare ground coverage over time—clustered at the downslope edge of the grove. NDVI decline across Transect C is statistically significant (r=-0.74, n=9, p=0.02); Transect A is marginally significant (r=-0.64, n=9 p=0.062) and D is insignificant (r=-0.67, p=0.33, n=4) which can be expected given their relatively low degrees of freedom. Regardless of statistical significance, all transects reveal a strong negative correlative relationship between position and NDVI change, as groves universally experience upslope growth overtime and declines on the downslope edges (mean r=-0.72, minimum r=-0.64).

Discussion

With climate change expected to result in increasing warming and drying trends on a global scale, each ecosystem will experience different consequences and adjustments (IPCC 2014). Our study area in the Eastern Colorado shortgrass steppe—representative of much of the North American arid grasslands—has already begun experiencing local regime shifts over the past two decades, trending warmer and drier (Nasvik 2021), and resulting in significant coverage loss of dominant *Bouteloua gracilis* (Rondeau et al. 2013). Previous studies at our Chico Basin Ranch site have suggested that the system is responding through developing banded vegetation patterns to increase water management efficiency (Nasvik 2021; Sticpewich 2022) however, the mechanisms for this self-organization were not known. The key result of our study indicates that this pattern is formed by distinct periodic strips of dying grass, which eventually erode to bare ground.

Aggregate data of transect surveys throughout the AOI reveal an overall directional trend for the system, which was once characterized by nearly full vegetation coverage just over a decade ago (Nasvik 2021). Currently, living grass remains in high coverage on the upslope edge of the groves with presence of senescing grass increasing through the downslope grove, and dead grass marking the transition to the intergrove which eventually gives way to bare ground (Fig. 6). This observed groundcover trend aligns with previous discussions of scale-dependent feedback surrounding self-patterning vegetation, describing how plants immediately downslope of the intergrove are the first to make use of incoming sheetflow and therefore water availability wanes as plants continuously uptake it as it moves downslope within the grove (Aguiar & Sala 1999; Rietkerk & van de Koppel 2008). Ultimately, this uneven water distribution limits the size of groves resulting in a heterogeneous, periodically spaced vegetation cover. Our analysis of change in NDVI from 2020 to 2023—representing health and density of the grass—reveals the progression of this scale-dependent feedback on a temporal scale, with a trend of growth along the upper edges of groves and decline in health or density along the downslope edges; relative magnitude of vegetation changes should be further studied to determine overall biomass changes in relation to patterning on this site.

Further analysis of individual transects' land cover makeup reveals several different stages of pattern development based on vegetation organization. This categorization aligns with previous studies on banded vegetation formation which found both a building and degenerative phase. The building phase describes vegetation increasingly establishing within a certain location, with the degenerative phase encompassing nearby loss of vegetation cover and associated degradation of soil mound microtopography formed by root structures (Aguiar & Sala 1999). Rondeau (2013) described a similar phased land cover transition associated with the loss of Blue grama cover at a nearby study site, in which decline in vegetation cover was initially countered by an increase in litter cover before reaching bare ground (though banded vegetation was not observed at this site during the researchers' study period). Our fine scale land cover data best captures the degenerative phase in stripe development, as Type I begins to see concentrated grass death interspersed with living grass, Type II advances to one distinct band of living grass and one bare, and Type III is marked by the erosion of dead grass heads into bare ground at bottom of the intergrove, which presumably have been dead the longest based on water movement.

Our results also indicate that both the building and degenerative phase of band formation will continue to persist through positive feedback loops. In the map of NDVI change from 2020 to 2023, it is clear that patterns of concentrated growth align with pre-existing groves, and concentrated health decline continues along areas which are already bare. The self-perpetuating trend of each microsite is expected since the presence of vegetation increases ability to maintain and use water though greater soil infiltration and shading to decrease evaporation, and bare patches contrastingly encourage surface flow (Dunkerly 2018). Specifically, crusty soil—which was observed at Chico Basin Ranch and has been known to form atop bare patches—can lock bands into a fixed position as it is very difficult for plants to re-establish upon it (Dunkerly 2018). Additionally, models have predicted long term trends in areas presenting spatial patterns to be increasingly challenging to reverse once established. A model by Rietkerk et al. (2002) found that the range of rainfall for which patterns are predicted widens with increasing plant mortality associated with the intergrove bands, and a model by Dunkerly (1997) found heightening water shortages resulted in increasingly isolated bands, with the most recovery occurring along pre-existing stripes once rainfall increased. While models certainly cannot entirely capture the complexities of a system, their predicted results of self-perpetuating spatial patterning are generally supported by both our results and the physiology of *Bouteloua gracilis* (yet our results do not indicate upslope movement of stripes at this time, which is commonly included in models).

As a cost of significant drought tolerance, the life history and physiology of Blue grama grass makes sexual reproduction very difficult, and therefore the species relies heavily on asexual reproduction via cloning and rhizomal development (Eneboe et al. 2002; Smith et al. 2004). C4 species' tendency to conserve water ultimately limits new growth via germination as seedlings are given limited water reserves and present less rigorous growth rates—particularly in times of stress—compared to C_3 species (Qi & Redmann 1993). While total biomass loss in conjunction with pattern formation over the past two decades has not been investigated at this site, it is reasonable to assume Blue grama biomass loss similar in magnitude to that observed at a study plot only 10 kilometers away by Rondeau (2013). The exact mechanism of grass death is unclear, but previous studies on Blue grama in the face of drought stress suggest a failure of drought recovery mechanisms following long-term lack of adequate water. An experimental study by

Lemoine et al. (2018) examined the ability of Blue grama individuals to recover after exposure to repeated severe drought within one growing season. The researchers found that while plants were able to recover previous photosynthesis rates following the first drought, that does not translate directly to productivity and they were unable to recover the biomass loss both during and following the recovery period, as biomass lags remained for several years. Therefore, the physiological consequences of repeated drought will be cumulative and when a second drought was imposed onto the plants, though their photosynthesis rates were depressed to a lesser extent than during the first experimental drought, it likely represents a stress-hardening strategy rather than physiological acclimation . This hardening response should increase drought tolerance but such resistance to desiccation may come at the expense of primary productivity throughout the following life cycle of the plant. Authors made this attribution based on their finding that plants experienced a similar magnitude of biomass loss resulting from a late-season drought whether it was their first or second drought of the season, and this milder response was because they had naturally reduced late-season growth rates and had little capacity for further biomass reduction. Additionally, in their analysis of Blue grama root dynamics under drought recovery, Lauenroth et al. (1987) suggest that Blue grama roots may be susceptible to desiccation and cell death under extremely dry soil conditions, which results in losing contact with the soil therefore greatly limiting the ability to quickly respond to precipitation pulses, a trait crucial to survival as the dominant species on arid grasslands. Regardless of the exact causes for reaching physiological limits, Evans et al. (2011) found that even with extreme drought resilience, established Blue grama communities can reach a stress tolerance threshold and will begin to die following prolonged drought exposure of nearly a decade, which is relevant to our study as it is the same time scale as our spatial reorganization. While these studies provide compelling arguments for the cumulative effects of repeated, long-term, and severe drought which likely compounded for the initial tipping point of death and reorganization at our study site, there appears to be an overall lack of literature surrounding the mechanisms of Blue grama death under prolonged and severe drought stress, which is crucial to understanding the future and recovery options for arid grassland sites. Based on our results, it is clear that the presence of dead grass bands leading to bare ground and apparent continuing development of this pattern over time reveals that once death does begin occurring in a certain area, it makes the surrounding microhabitat less suitable for others, in turn perpetuating trends of death and spatial reorganization.

With the loss of adult individuals in large areas and spatial feedback systems limiting the growth of groves via asexual production, sexual reproduction becomes crucial for regaining homogenous cover, yet the potential habitats under a heterogeneous banded regime likely limit seedling establishment. Active root biomass of Blue grama grass is 90% concentrated within the upper 30 centimeters of soil as they rely heavily on widespread below-surface adventitious roots to quickly absorb incoming precipitation. Since adventitious roots grow so close to the surface during seedling development, they are especially susceptible to desiccation from overly dry soil (Aguilera & Lauenroth 1993). As a consequence of adult Blue grama plants' extreme efficiency in uptaking water for themselves, seedlings are typically unable to establish in close proximity to adult neighbors; Aguilera & Lauenroth (1993) experimentally found that greater distance and overall isolation from adult neighbors resulted in greater establishment success. Despite Blue grama seedlings success with isolation from adult plants, the intergroves' highly reduced ability to maintain water—specifically within the top five centimeters of soil which is most important for root development—also presents an unsuitable habitat for establishment, and seedlings

typically avoid the location of their predecessors (i.e. dead grass heads) due to remaining root structures (Aguilera & Lauenroth 1993; Aguilera & Lauenroth 1995). Therefore, the typical gaps between grass hummocks of Blue grama populations provides crucial microhabitats for seedlings, which can enjoy the general water-maintenance benefits of the population but without intense below-ground competition from immediate neighbors (Joern & Mole 2005; Aguilera & Lauenroth 1993). Once individuals establish adventitious roots, they are able to fully benefit from the facilitation of close neighbors but establishing seedlings must strike a careful balance between community facilitation and inhibition during their most vulnerable period (Aguilera & Lauenroth 1993); this tight margin is especially critical if groves are becoming increasingly dense to account for lost biomass in intergroves, therefore providing even less suitable habitat for sexual reproduction. Given these factors, most establishment is likely very limited to the upper edge of groves—where this study found the most growth from 2020 to 2023—and where seedlings receive the most incoming water from the intergroves with limited interference from adult neighbors, but still receive environmental shading and increased infiltration associated with established communities.

Blue grama grass accounts for approximately 90% of plant cover and annual primary production in the North American shortgrass steppe (Lemoine at al. 2018). It is one of the most resilient and important grazing species on the Great Plains, and even if replaced, the disappearance of this population presents significant implications for agriculture since incoming species are often less nutritious (Rondeau et al. 2017). Therefore, any reaction to climate change as drastic as that occurring at Chico Basin Ranch is worth noting and further investigating. Blue grama grass is also one of the most drought-resilient prairie species (Rondeau 2013), yet emergent banding patterns signify that it has reached a water-availability tipping point which could stand precariously near the collapse of the system (Rietkerk & van de Koppel 2008). Further research centering on blue grama drought stress physiology, senescence, and the resilience of pattern development prior to collapse must be completed to fully understand the mechanisms of periodic death which drive this pattern formation. Monitoring efforts should also be made using aerial imagery similarly as that demonstrated in this study in order to hear and answer the warning call being made by this critical ecosystem in the face of an increasingly-threatening climate.

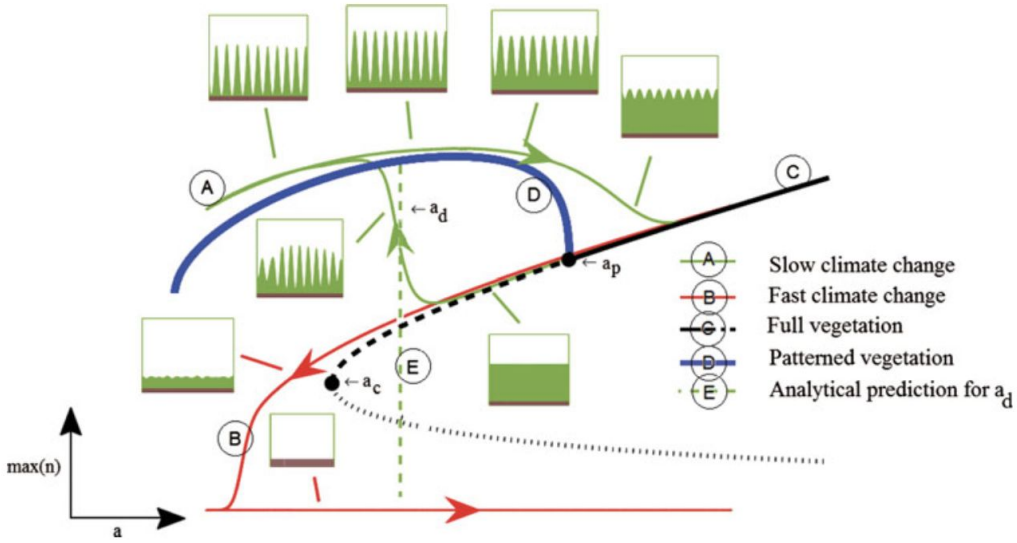

Figure 1. Schematic demonstrating the evolution of vegetation patterns under differing progressions of climate change. The green curve A under a slowly-transitioning climate avoids the tipping point by transitions to a patterned state (assuming the blue curve D). The red curve B under fast climate change does not have time to respond and advances towards ecosystem collapse. Values of a below a_p and above a_c (dashed black curve C) still maintain full vegetation, but are unstable to disturbances. We suppose our study site exists on the green curve A, which has adequate time to adopt a patterned vegetation state in response to water shortages. Figure adopted from Chen et al. Figure 1.

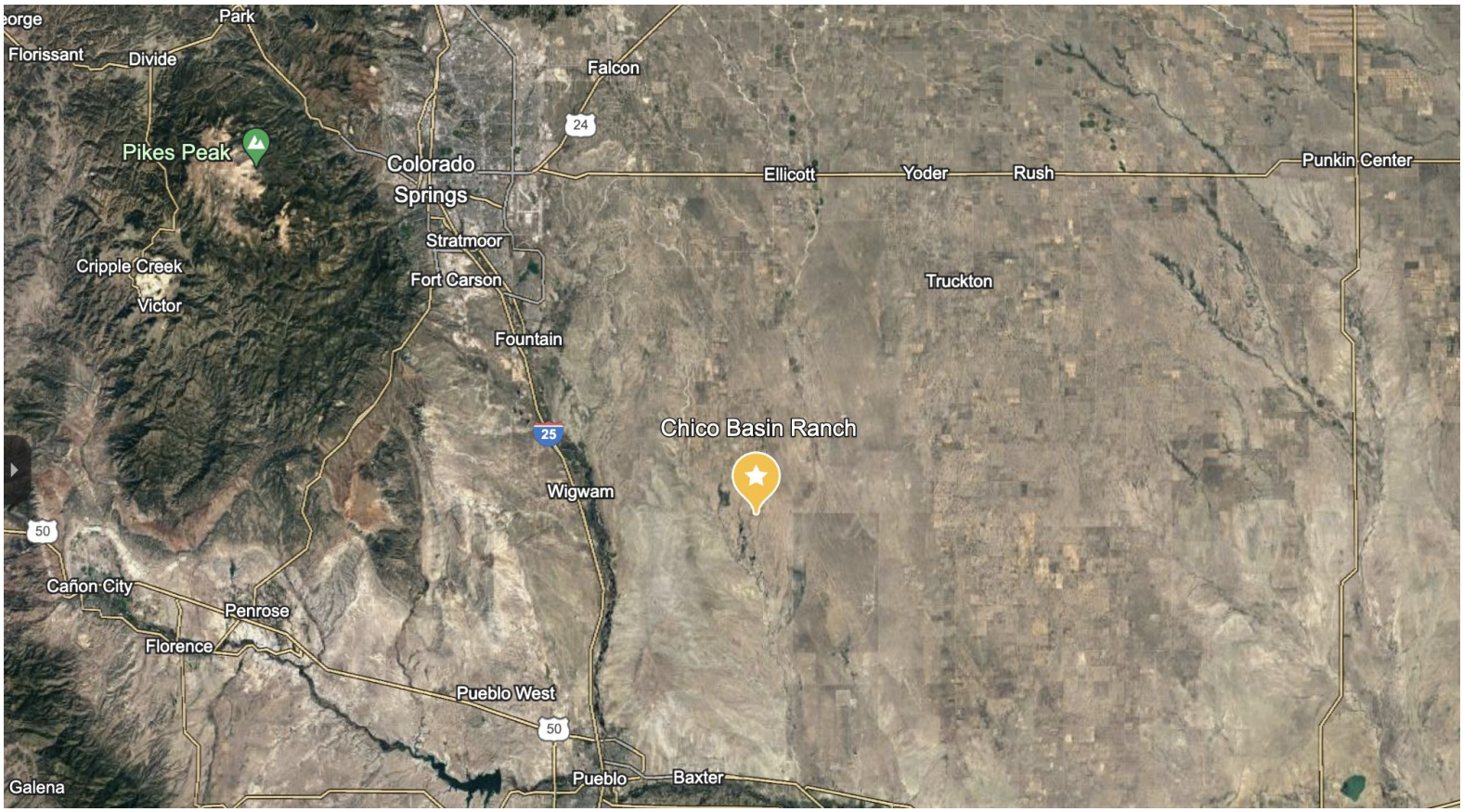

Figure 2. Our study site at Chico Basin Ranch (coordinates: 38.5131833˚, -104.4222770˚) located between Colorado Springs and Pueblo, CO, east of the Tava (Pikes Peak) region of the Rocky Mountains. This landscape marks a stark transition between mountain range foothills and flat, arid grasslands. Image captured from Google Earth (attributed 10/17/2019).

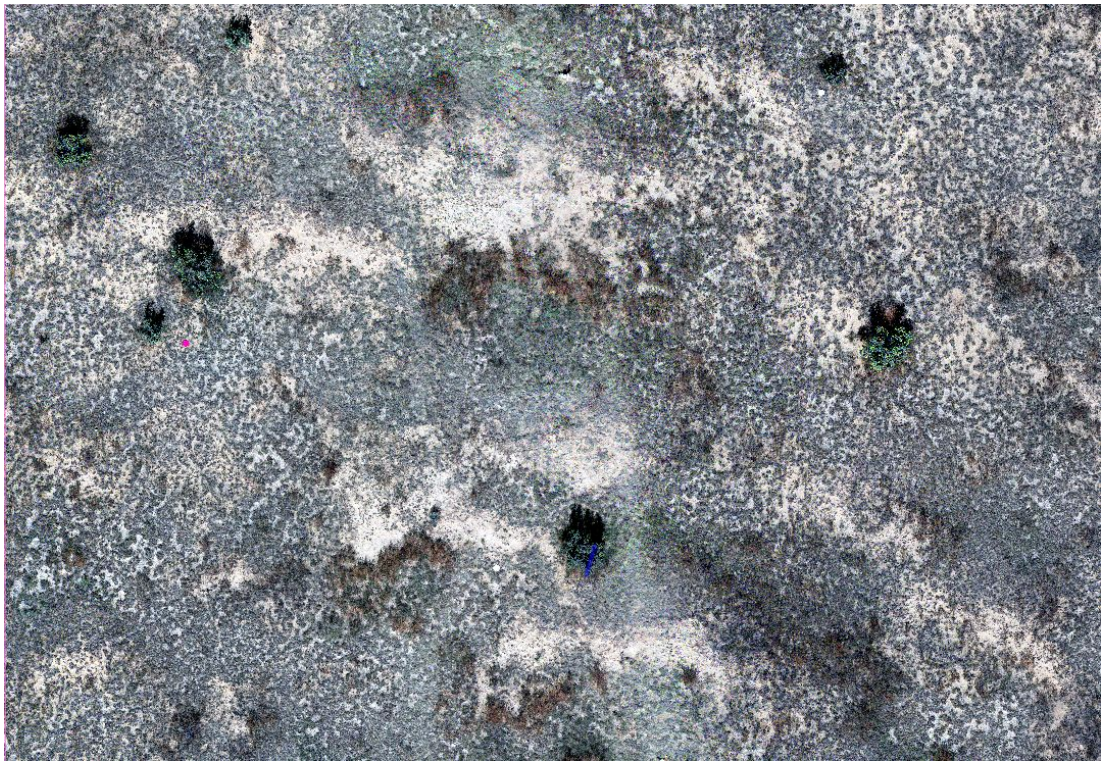

Figure 3. Area of interest for aerial image analysis. This 29 meter x 43 meter plot was selected for its concentration of several well-defined bands and several large cacti for geolocation.

(a)

(b)

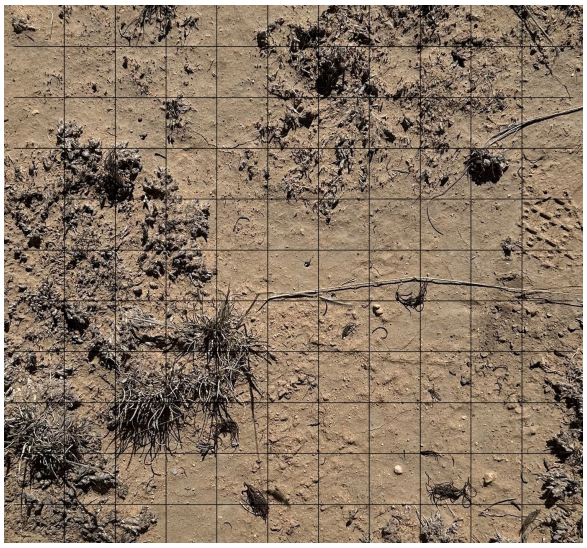

(c)

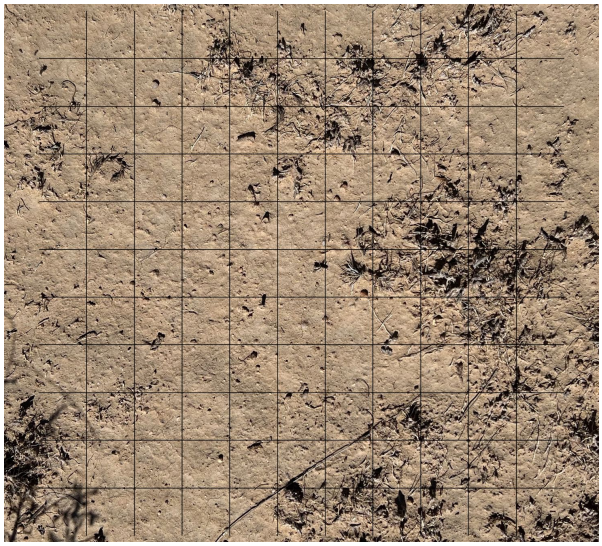

Figure 4a-c. Example quadrat photos with 11x11 grids overlaid for land cover surveying. A is representative of a quadrat dominated by living grass (commonly found at the upslope edge of groves), B contains mostly dead heads (upslope of intergrove) of grass, and C is a quadrat of mostly bare ground (downslope intergrove).

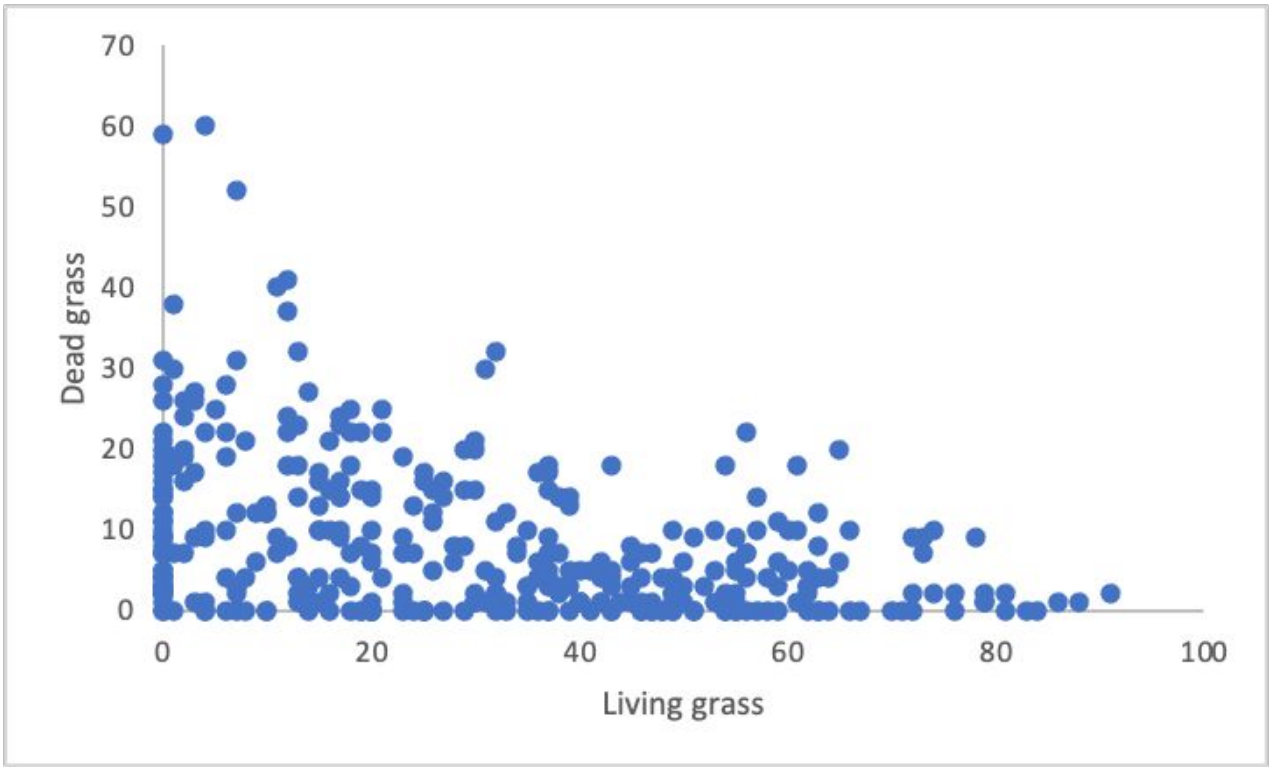

Figure 5. Living grass coverage plotted against the number of dead grass heads for all transects. This plot reveals an envelope correlation between the two land cover types, in which there are instances where there is neither dead or living grass or a small proportion of both, but they do not co-exist in high densities. This relationship is statistically significant (-0.386, n=373,p=1.211e-14).

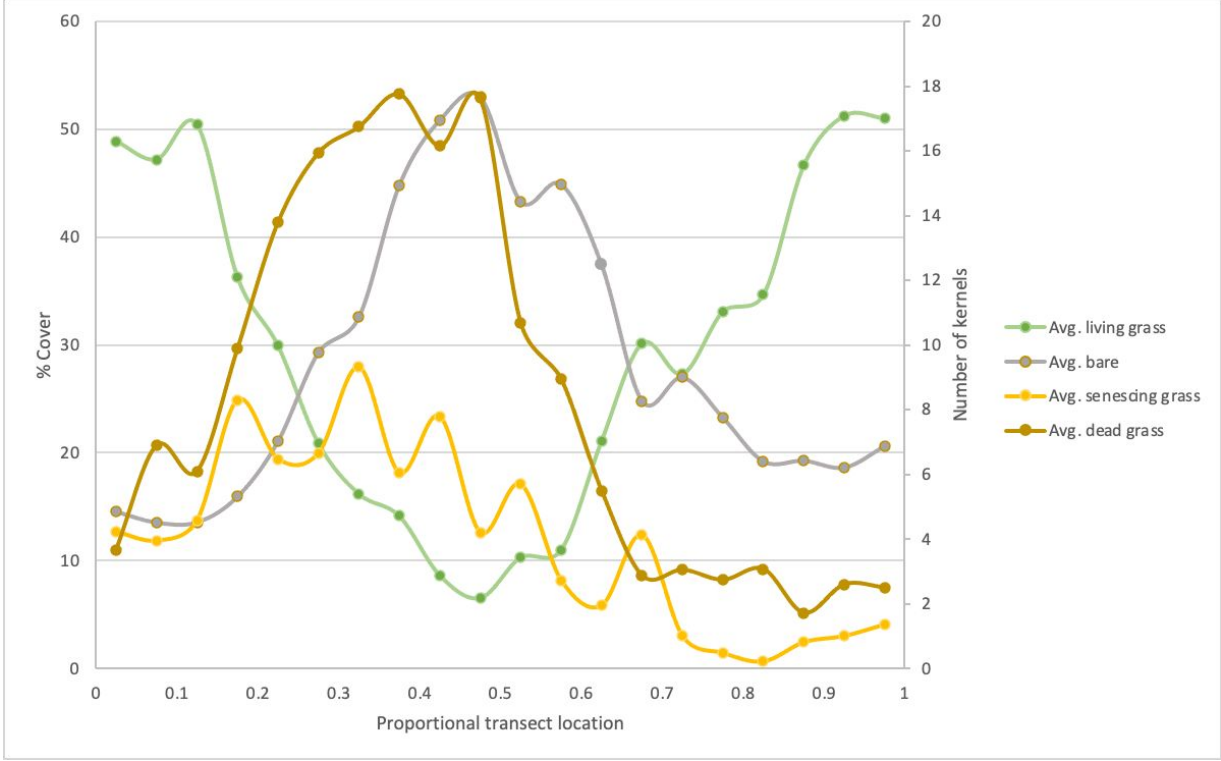

Figure 6. Aggregate plot of average land cover type throughout all transects plotted along a normalized proportional transect distance. Average living grass and bare ground are plotted on the left y-axis as percent coverage, and dead grass and senescing grass are plotted on the right y-axis as number of kernels.

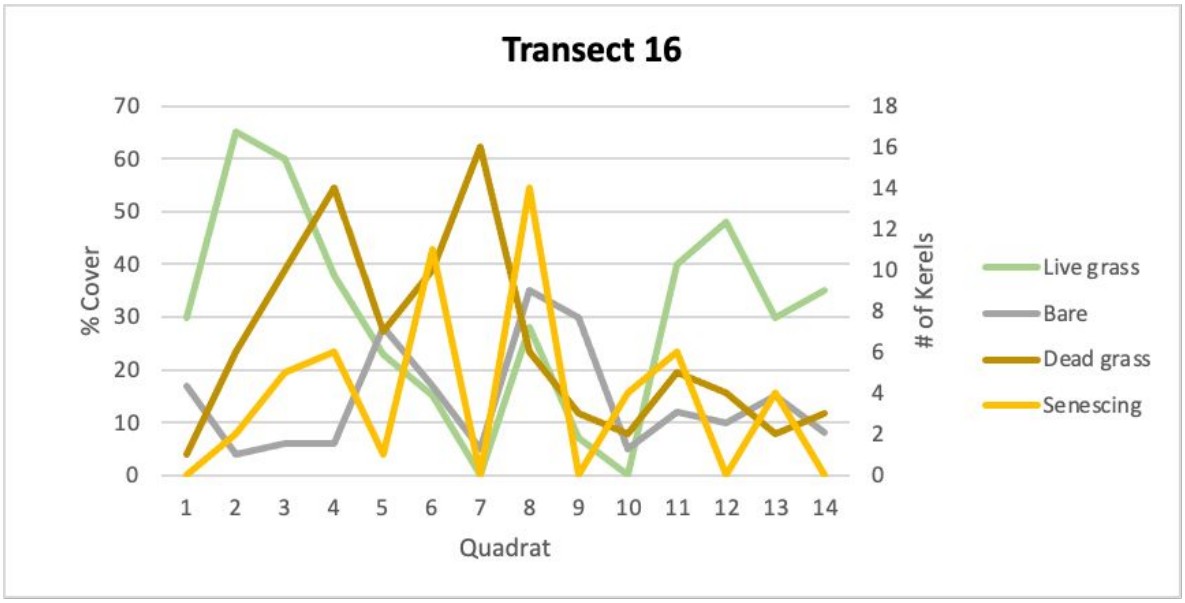

(a)

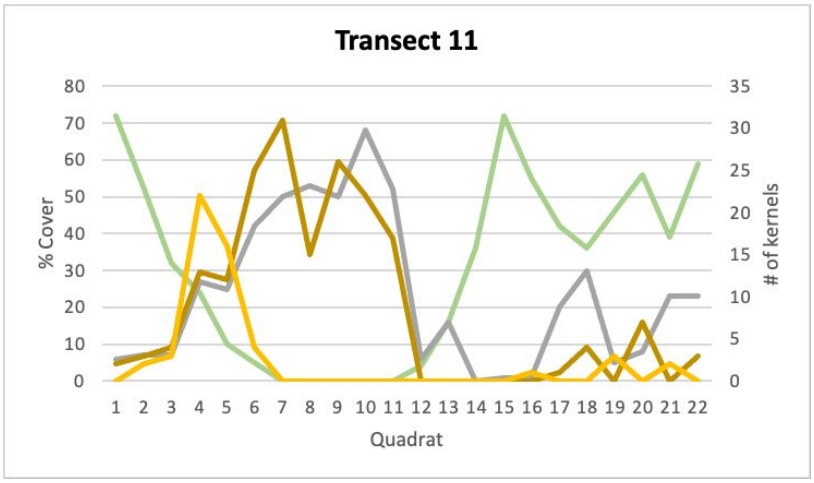

(b)

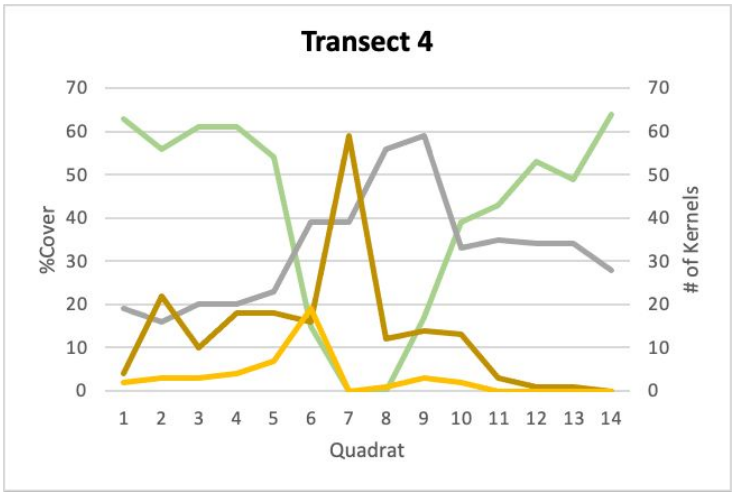

(c)

Figure 7a-c. Representative plots of living, dead, and bare grass across transects displaying three stages of pattern development. Percent cover of living grass and bare ground are plotted on the left y-axis, and number of dead or senescing grass kernels is plotted on the right y-axis. Type I (a) displays a generally inverse relationship between dead and living grass, but patches primarily living or dead are spatially interspersed. Type II (b) displays a strongly inverse relationship between living and dead grass, with a distinct section in which dead grass dominates over living but still retains coverage. Type III (c) has the same inverse relationship between living and dead grass, with a primarily bare patch on the downslope edge of the intergrove. See Appendix 2 for plots of all transects.

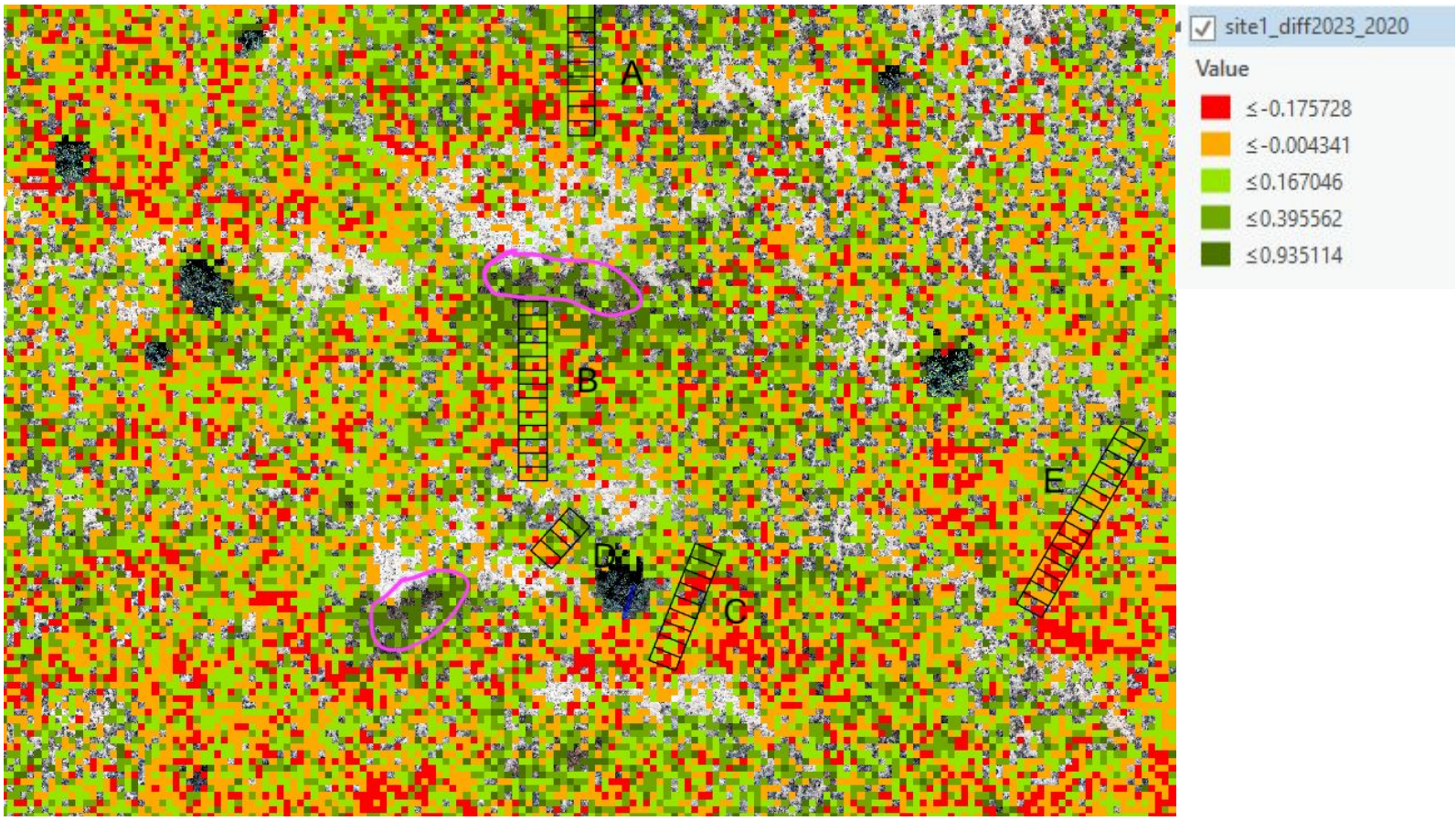

Figure 8. Map of NDVI change in the AOI from 2020 to 2023, with labeled transects for statistical analysis. Red and orange pixels represent areas in which NDVI has decreased (less than 0), and different shades of green represent areas in which NDVI has increased (greater than 0). 3 out 5 transects display a statistically significant relationship between NDVI change over the past three years and location within the transect, with the upslope edge of groves increasing in greenness and downslope edges decreasing; all transects has strong negative correlations regardless of significance (mean r=-0.72, minimum r=-0.64). Dense tumbleweed growth which could be removed is outlined in pink.

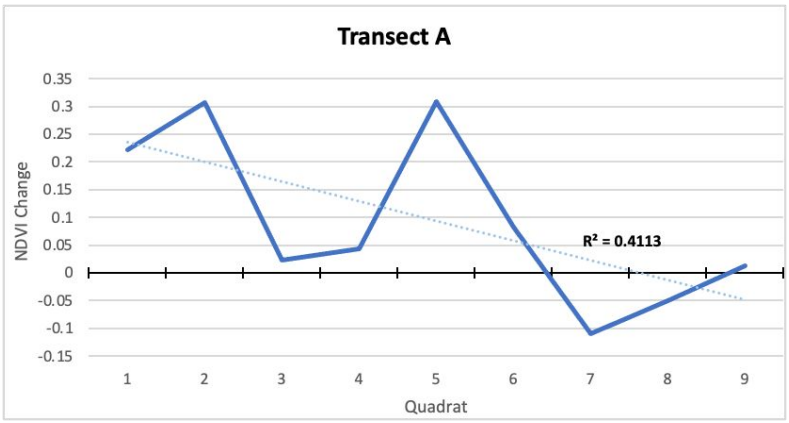

(a)

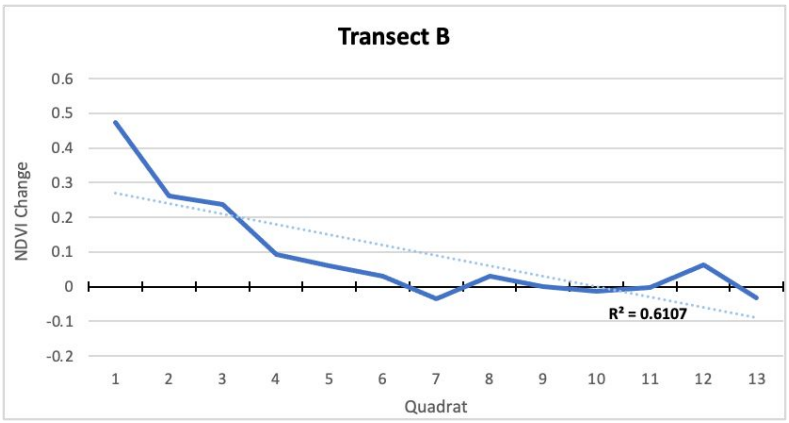

(b)

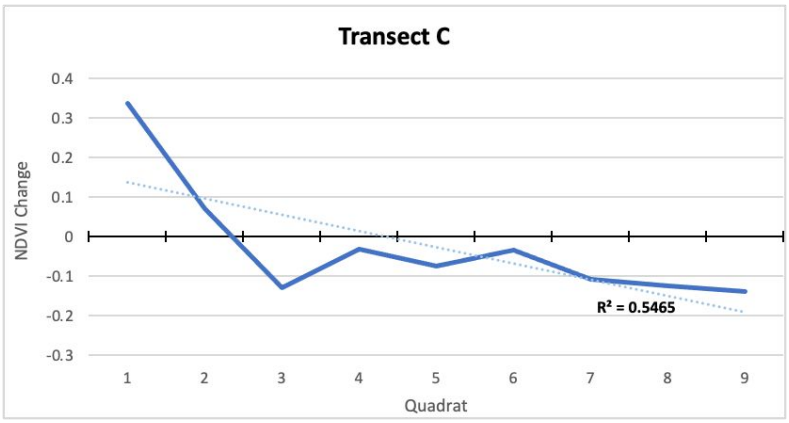

(c)

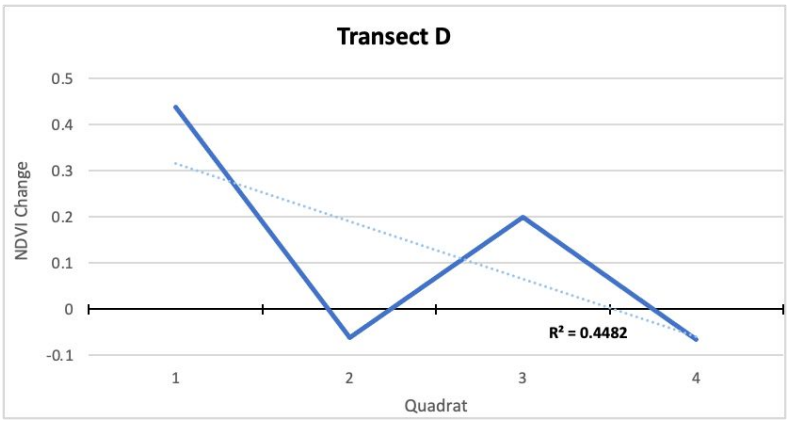

(d)

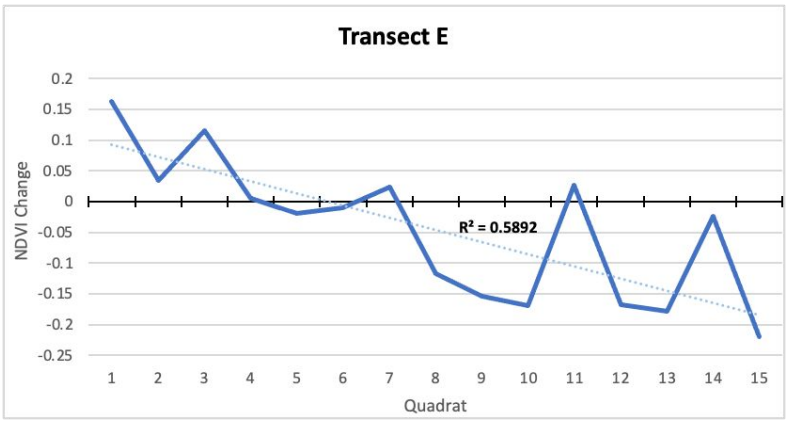

(e)

Figure 9a-e. NDVI change from 2020 to 2023 plotted over several groves, as outlined by their respective transects in Figure 8. Each transect displays a downward trend in NDVI, as positive values in the beginning of the transect (and its associated grove) represent increasing grass health or density, with negative values at the bottom indicating declining health or density. Transects B, C, and E are statistically significant in this trend ($p<0.5$), and Transect A is marginally significant (see Table 2 for full statistics).

Tables

	Living grass-Senescent grass			Senescent grass-Dead grass			Dead grass-Bare ground		
Lag	**r**	**p**	**df**	**r**	**p**	**df**	**r**	**p**	**df**
0	-0.42763	0.06000	18	0.79542	*2.76137e-05	18.00000	0.64938	*0.00195	18
1	-0.16237	0.50662	17	**0.91777**	**3.12438e-08	17.00000	0.81518	*2.11993e-05	17
2	0.10731	0.67169	16	0.82701	*2.30698e-05	16.00000	**0.92719**	**3.15492e-08	16
3	0.42252	0.09110	15	0.75238	*0.00049	15.00000	0.91443	*2.80690e-07	15
4	0.60730	0.01259	14	0.52711	*0.03590	14.00000	0.72704	*0.00142	14
5	0.73564	0.00177*	13	0.32127	0.24297	13.00000	0.41291	0.12610	13
6	**0.87197**	***4.79891e-05	12	0.12864	0.66118	12.00000	0.02115	0.94280	12
7	0.86994	0.00011*	11	-0.14019	0.64782	11.00000	-0.42770	0.14488	11

Table 1. Lag correlation table of average peak location for adjacent land cover types on a spatially normalized transect; each lag represents 10% of the normalized transect difference . Statistically significant p-values are starred (*), and the lag with the greatest p-value for each pair is starred (**) and bolded with the corresponding r-value.

Transect	r	p	n
A	-0.64	0.062*	9
B	-0.78	0.001***	13
C	-0.74	0.02***	9
D	-0.67	0.33	4
E	-0.77	0.00083***	15

Table 2. Correlation table for each transect (A-E) on the NDVI change map from 2020 to 2023 (Fig. 8). All transects reveal a negative r-value with NDVI change shifting from positive to negative down the transect. The transects were divided into bins (n) from which average NDVI change was calculated at different sections along the transect. Three transects had statistically significant p-values (***) and a fourth was marginally significant (*).

References

Aguilera, M. O., & Lauenroth, W. K. (1993). Seedling establishment in adult neighbourhoods--Intraspecific constraints in the regeneration of the bunchgrass Bouteloua gracilis. *Journal of Ecology*, 253-261.

Aguilera, M. O., & Lauenroth, W. K. (1995). Influence of gap disturbances and type of microsites on seedling establishment in Bouteloua gracilis. *Journal of Ecology*, 87-97.

Aguiar, M. R., & Sala, O. E. (1999). Patch structure, dynamics and implications for the functioning of arid ecosystems. *Trends in Ecology & Evolution*, *14*(7), 273-277.

Chen, Y., Kolokolnikov, T., Tzou, J., & Gai, C. (2015). Patterned vegetation, tipping points, and the rate of climate change. *European Journal of Applied Mathematics*, *26*(6), 945-958.

Colorado Climate Center. Colorado State University.

Dunkerley, D. L. (1997). Banded vegetation: survival under drought and grazing pressure based on a simple cellular automaton model. *Journal of Arid Environments*, *35*(3), 419-428.

Dunkerley, D. (2018). Banded vegetation in some Australian semi-arid landscapes: 20 years of field observations to support the development and evaluation of numerical models of vegetation pattern evolution. *Desert*, *23*(2), 165-187.

Eneboe, E. J., Sowell, B. F., Heitschmidt, R. K., Karl, M. G., & Haferkamp, M. R. (2002). Drought and grazing. IV. Blue grama and western wheatgrass. *Rangeland Ecology & Management/Journal of Range Management Archives*, *55*(2), 197-203.

Evans, S. E., Byrne, K. M., Lauenroth, W. K., & Burke, I. C. (2011). Defining the limit to resistance in a drought‐tolerant grassland: long‐term severe drought significantly reduces the dominant species and increases ruderals. *Journal of Ecology*, *99*(6), 1500-1507.

IPCC (2014). Summary for policymakers. In: Field CB, Barros V, Stocker TF et al (eds) Managing the risks of extreme events and disasters to advance climate change adaptation. A special report of working groups I and II of the Intergovernmental Panel on Cli- mate Change. Cambridge University Press, Cambridge, pp 1–19.

Joern, A., & Mole, S. (2005). The plant stress hypothesis and variable responses by blue grama grass (Bouteloua gracilis) to water, mineral nitrogen, and insect herbivory. *Journal of chemical ecology*, *31*, 2069-2090.

Lauenroth, W. K., Sala, O. E., Milchunas, D. G., & Lathrop, R. W. (1987). Root dynamics of Bouteloua gracilis during short-term recovery from drought. *Functional Ecology*, 117-124.

Lemoine, N. P., Griffin-Nolan, R. J., Lock, A. D., & Knapp, A. K. (2018). Drought timing, not previous drought exposure, determines sensitivity of two shortgrass species to water stress. *Oecologia*, *188*, 965-975.

Nasvik, Sophie (2021). Statistical analysis of banded periodic patterns in arid grasslands. Unpublished manuscript. Department of Environmental Sciences, Colorado College.

Noy-Meir, I. (1973). Desert ecosystems: environment and producers. *Annual review of ecology and systematics*, *4*(1), 25-51.

Qi, M. Q., & Redmann, R. E. (1993). Seed germination and seedling survival of C3 and C4 grasses under water stress. *Journal of Arid Environments*, *24*(3), 277-285.

Rietkerk, M., Boerlijst, M. C., van Langevelde, F., HilleRisLambers, R., de Koppel, J. V., Kumar, L., ... & de Roos, A. M. (2002). Self-organization of vegetation in arid ecosystems. *The American Naturalist*, *160*(4), 524-530.

Rietkerk, M., Dekker, S. C., De Ruiter, P. C., & van de Koppel, J. (2004). Self-organized patchiness and catastrophic shifts in ecosystems. *Science*, *305*(5692), 1926-1929.

Rietkerk, M., & Van de Koppel, J. (2008). Regular pattern formation in real ecosystems. *Trends in ecology & evolution*, *23*(3), 169-175.

Rondeau, R. J. (2013). Vegetation response in a Colorado grassland-shrub community to extreme drought: 1999–2010. *The American Midland Naturalist*, *170*(1), 14-25.

Rondeau, R. J., Decker, K. L., & Doyle, G. A. (2017). Potential consequences of repeated severe drought for shortgrass steppe species. *Rangeland Ecology & Management*, *71*(1), 91-97.

Sims, P. L., Lang'at, R. K., & Hyder, D. N. (1973). Developmental morphology of blue grama and sand bluestem. Journal of Range Management, 26(5), 340-344.

Smith, S. E., Haferkamp, M. R., & Voigt, P. W. (2004). Gramas. *Warm‐Season (C4) Grasses*, *45*, 975-1002.

Sticpewich, Haidee (2022). Microhydrology of a periodically-patterned arid grassland: surface water dynamics, infiltration, and soil water accumulation in a simulated rainfall experiment. Unpublished manuscript. Department of Environmental Sciences, Colorado College.

Turing, A. M. (1952). The chemical basis of morphogenesis. *Bulletin of mathematical biology*, *52*, 153-197.

Appendices

Appendix 1. Lag correlation R-Script

Lag between dead grass and bare ground peaks

```
lags<-8 #max number of shifts of the dataset
r.table<-matrix (nrow=lags, ncol=4, data=0);colnames(r.table)<-c("lag","r","p","df"); r.table[,1]<-0:(lags-1)
#little table that will be filled out in each loop and then we will choose the row with the highest r and stick it into the appropriate spot in the output

x<-data$DG
y<-data$BARE

for (i in 1:lags){
  a<-cor.test(x,y)
  r.table[i,2]<- as.numeric(a[4])
  r.table[i,3]<-as.numeric(a[3]) #p
  r.table[i,4]<- as.numeric(a[2])#df
  x<-data$DG[1:(20-i)]
  y<-data$BARE[(i+1):20]
}

r.table
plot(r.table[,1], r.table[,2], type="l")
write.csv(r.table, file="//Users/paigesimenz/Desktop/Thesis/results/DG_bare_lag.csv", row.names = FALSE)
```

Lag between senescent grass and dead grass peaks

```
lags<-8 #max number of shifts of the dataset
 r.table<-matrix (nrow=lags, ncol=4, data=0);colnames(r.table)<-c("lag","r","p","df"); r.table[,1]<-0:(lags-1)
#little table that will be filled out in each loop and then we will choose the row with the highest r and stick it into the appropriate spot in the output

 x<-data$SCEN
 y<-data$DG

 for (i in 1:lags){
   a<-cor.test(x,y)
   r.table[i,2]<- as.numeric(a[4])
   r.table[i,3]<-as.numeric(a[3]) #p
   r.table[i,4]<- as.numeric(a[2])#df
   x<-data$SCEN[1:(20-i)]
   y<-data$DG[(i+1):20]
 }

 r.table
 plot(r.table[,1], r.table[,2], type="l")
 write.csv(r.table, file="//Users/paigesimenz/Desktop/Thesis/results/SCEN_DG.csv", row.names = FALSE)
```

Lag between livings grass and senescent grass peaks

```
lags<-8 #max number of shifts of the dataset
 r.table<-matrix (nrow=lags, ncol=4, data=0);colnames(r.table)<-c("lag","r","p","df"); r.table[,1]<-0:(lags-1);
#little table that will be filled out in each loop and then we will choose the row with the highest r and stick it
into the appropriate spot in the output

 x<-data$LG
 y<-data$SCEN

 for (i in 1:lags){
   a<-cor.test(x,y)
   r.table[i,2]<- as.numeric(a[4])
   r.table[i,3]<-as.numeric(a[3]) #p
   r.table[i,4]<- as.numeric(a[2])#df
   x<-data$LG[1:(20-i)]
   y<-data$SCEN[(i+1):20]
 }

 r.table
 plot(r.table[,1], r.table[,2], type="l")
 write.csv(r.table, file="//Users/paigesimenz/Desktop/Thesis/results/LG_scen_lag.csv", row.names = FALSE
```

Appendix 2. Land cover plots: all transects sorted by level of pattern development

a. Type I "messy" transects

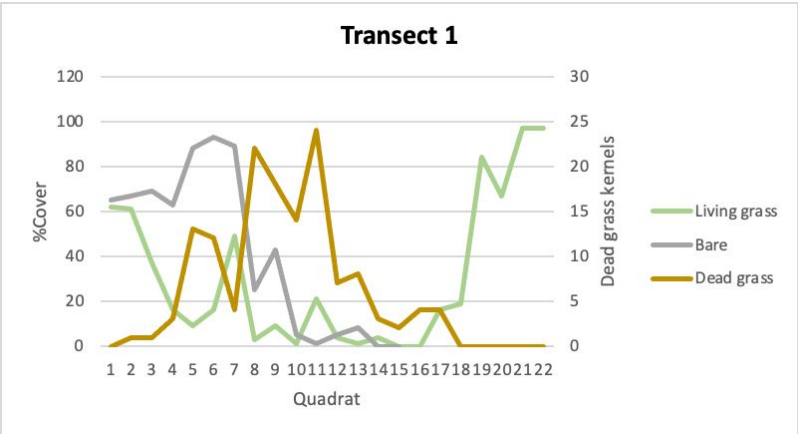

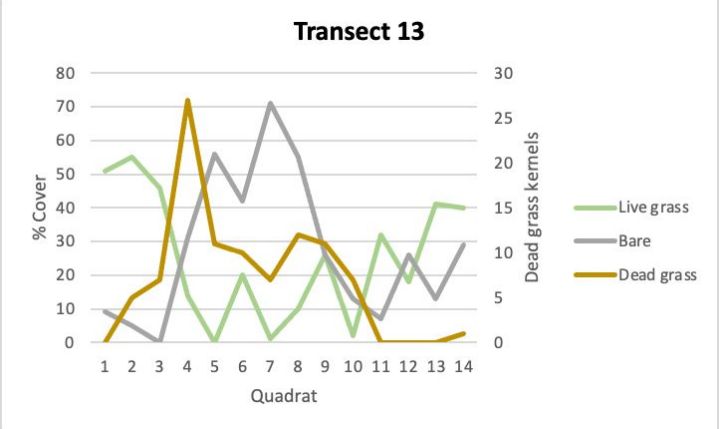

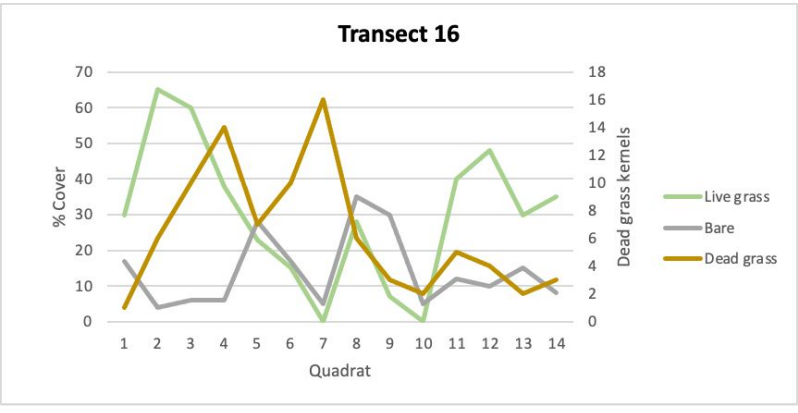

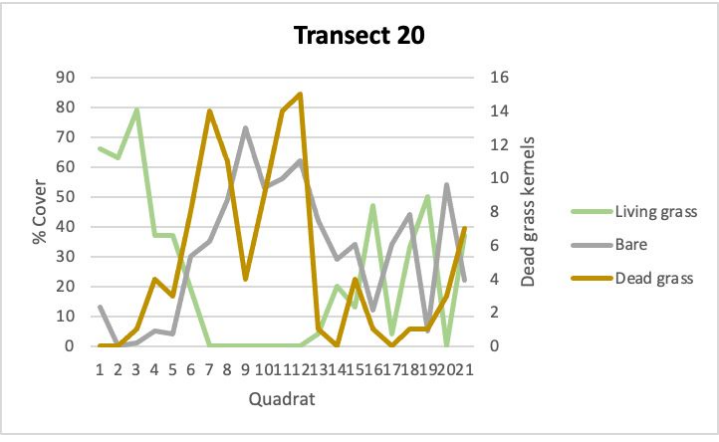

b. Type II "ordered" transects

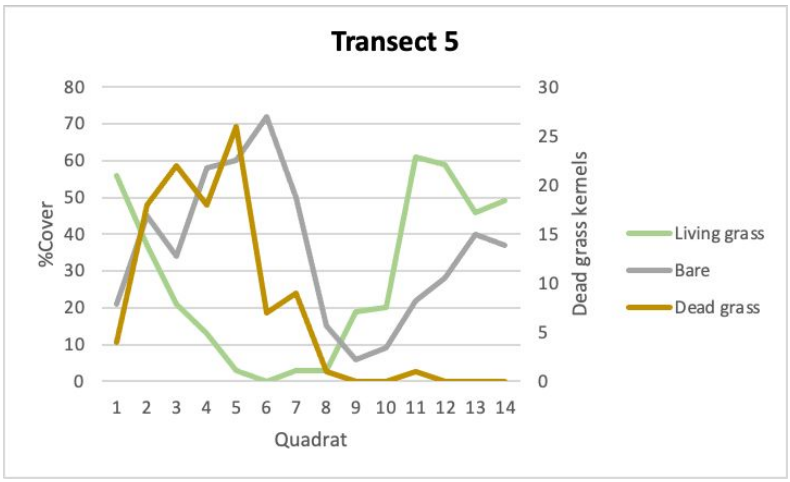

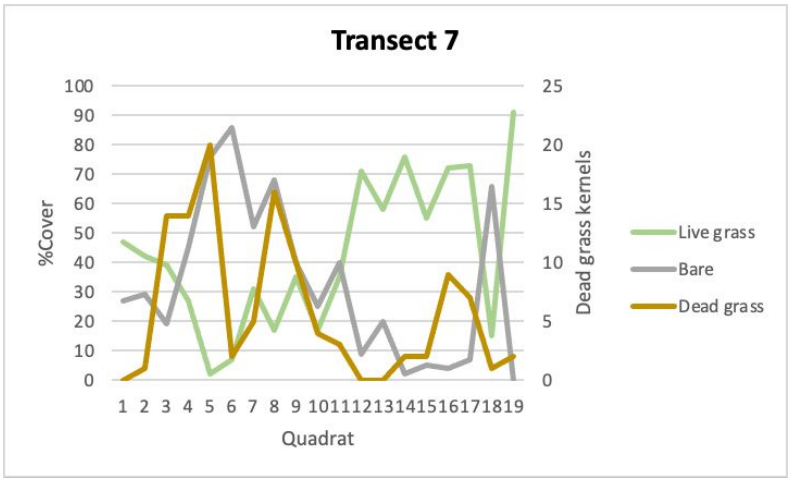

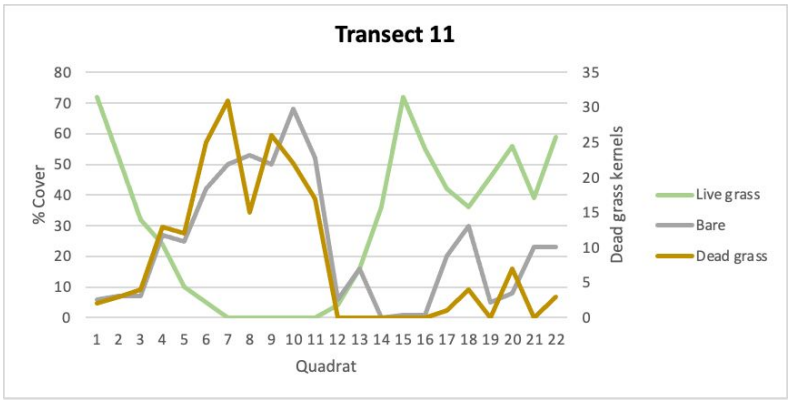

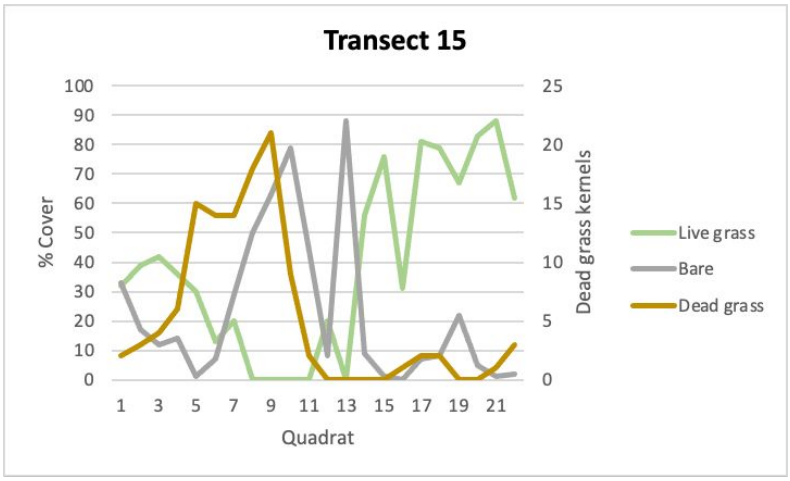

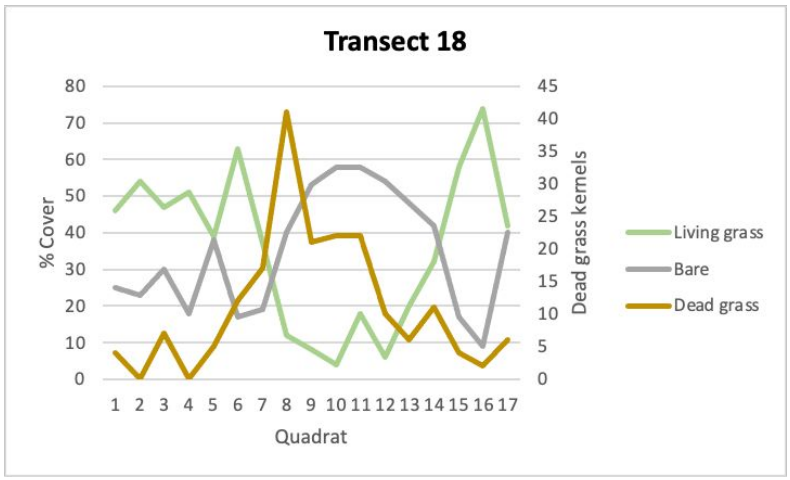

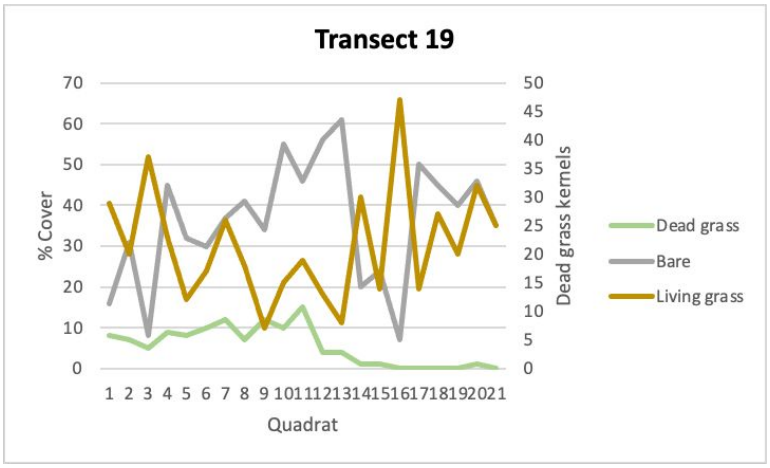

c. Type III "bare patch" transects

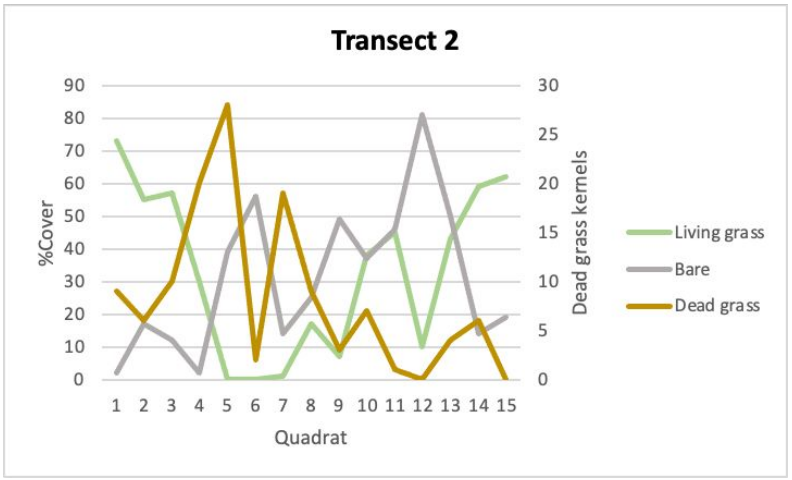

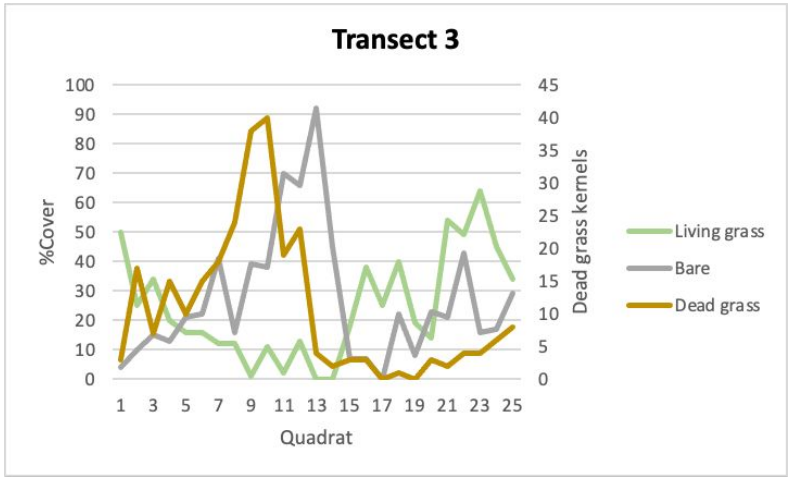

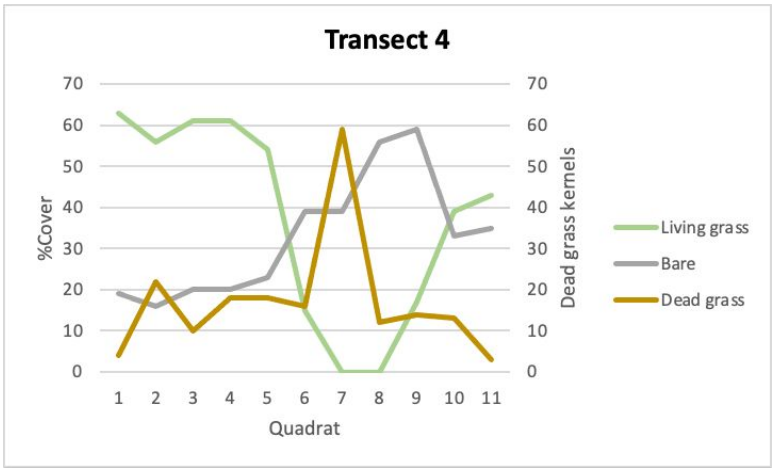

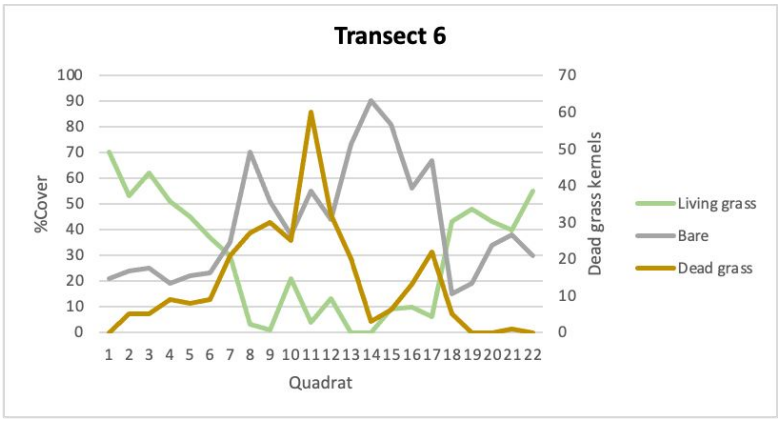

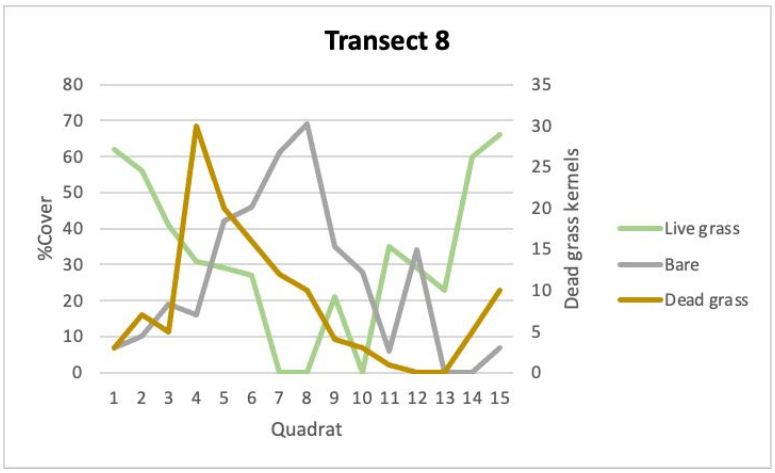

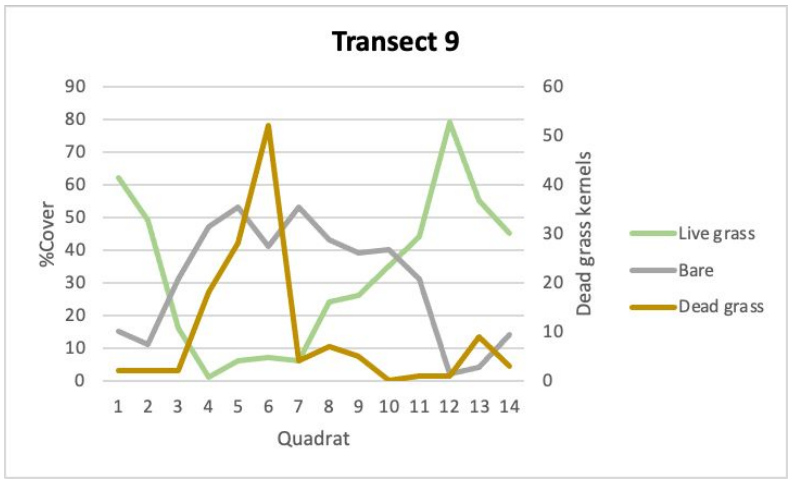

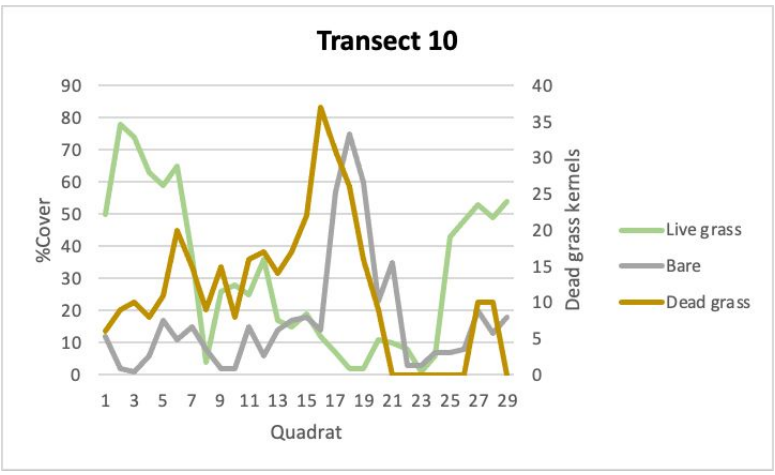

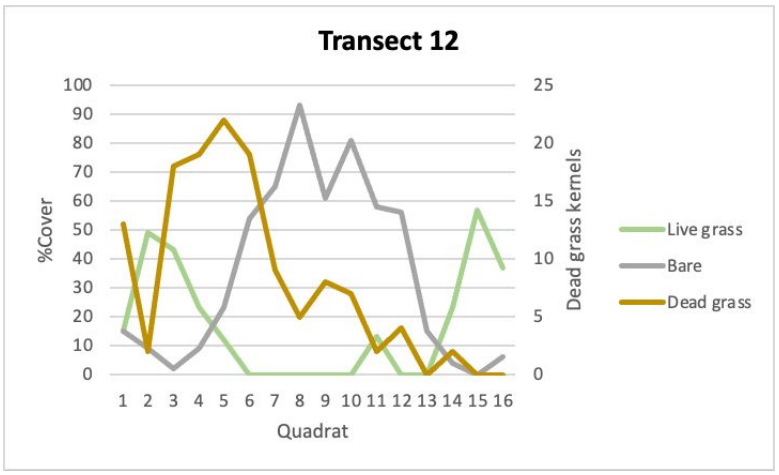

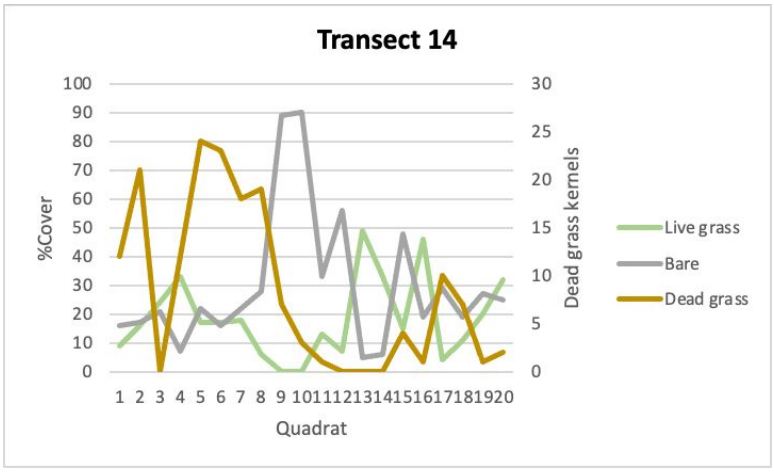
Transect 14
%Cover
Dead grass kernels
Quadrat
Live grass
Bare
Dead grass

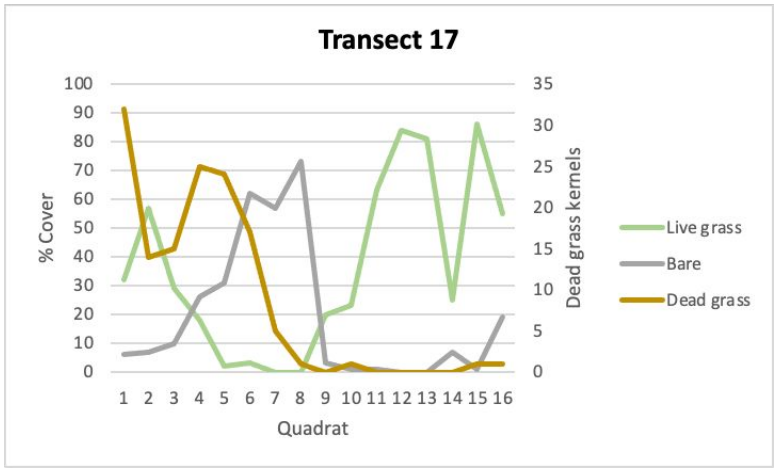
Transect 17
% Cover
Dead grass kernels
Quadrat
Live grass
Bare
Dead grass